universität wien

MASTERARBEIT / MASTER'S THESIS

Titel der Masterarbeit / Title of the Master's Thesis

„Computation of the ionic contribution to polarisability in solids“

verfasst von / submitted by

Nikolaus Martin Kandolf, BSc

angestrebter akademischer Grad / in partial fulfilment of the requirements for the degree of

Master of Science

Wien, 2018 / Vienna, 2018

Studienkennzahl lt. Studienblatt / degree programme code as it appears on the student record sheet:	A 066876
Studienrichtung lt. Studienblatt / degree programme as it appears on the student record sheet:	Master Physik
Betreut von / Supervisor:	Univ.-Prof. Dipl.-Ing. Dr. Georg Kresse
Mitbetreut von / Co-Supervisor:	Dr. Menno Bokdam

Contents

Abstract

The accurate description of ionic contributions to the frequency-dependent polarisability of a solid is essential for the understanding of optical phenomena in a wide range of materials. While the calculation of the ionic dielectric function at the DFT groundstate has become a routine task in electron structure theory, there is no standard method to describe the ionic polarisability at higher temperatures. This is particularly relevant for systems such as perovskite crystals, whose structures are notoriously unstable (dynamically stable), and exhibit a series of phase transitions between the groundstate and room temperature.

In this thesis, we investigate a statistical-mechanical approach to simulate the ionic dielectric properties of two perovskite systems, barium titanate and strontium titanate, at zero and non-zero temperatures. By means of the fluctuation-dissipation theorem, we derive an expression for the Kubo-Green relation of the ionic polarisability. According to this Kubo-Green relation, the polarisability can be expressed in terms of a time-correlation function of the total dipole fluctuations in a canonical ensemble at a set temperature T$>$0K.

Furthermore, we present a special case of a Kubo-Green relation which leads to significant reduction in the computational demands for low but non-zero temperatures, and we show that we can recover the standard formula for the groud-state polarisability as a limiting case of Kubo-Green.

All three presented methods are then applied to a series of test systems. We give a proof of principle with the example of the very stable α-SiO_2. In addition, we show the effectiveness of our approach by computing the finite-temperature polarisability of barium titanate and strontium titanate.

Zusammenfassung

Die genaue Beschreibung der ionischen Beiträge zur frequenzabhänigen Polarisierbarkeit eines Festkörpers ist grundlegend für ein Verständnis von optischen Phänomenen für viele verschiedene Materialien. Während Berechnungen der ionischen dielektrischen Funktion im DFT-Grundzustand mittlerweile routinemäßig durchgeführt werden, gibt es noch keine Standardmethode für die Beschreibung der ionischen Polarisierbarkeit bei höheren Temperaturen. Insbesondere für die Modellierung der strukturell sehr instabilen (dynamisch stabilen) Perowskitkristalle ist dieser Unterschied von höchster Relevanz, da diese Kristalle bei der Erwärmung auf Zimmertemperatur mehrere Phasenübergänge aufweisen, durch die die ionische Polarisierbarkeit stark beeinflusst wird.

In dieser Arbeit präsentieren wir einen statistisch-mechanischen Zugang zur Modellierung der ionischen dielektrischen Eigenschaften von zwei Perowskitsystemen, Bariumtitanat und Strontiumtitanat, im Grundzustand und bei höheren Temperaturen. Mittels des Fluktuations-Dissipations-Theorems leiten wir einen Ausdruck für die Kubo-Green-Beziehung der ionischen Polarisierbarkeit ab. Gemäß dieser Kubo-Green-Beziehung lässt sich die Polarisierbarkeit mittels einer Zeit-Korrelationsfunktion der Fluktuationen des Gesamtdipols in einem kanonischen Ensemble mit Temperatur $T>0$ beschreiben.

Weiters diskutieren wir einen Spezialfall der Kubo-Green-Beziehung, der eine signifikante Reduktion des Rechenaufwands für niedrige (aber finite) Temperaturen erlaubt, und wir zeigen dass die Standardformel für die Polarisierbarkeit im Grundzustand als Grenzfall von Kubo-Green erhalten werden kann.

Alle drei vorgestellten Methoden werden an Testsystemen ausprobiert. Mit dem bis zu sehr hohen Temperaturen stabilen α-Quartz (α-SiO_2) können wir die prinzipielle Richtigkeit der Ableitung darstellen. Darüber hinaus zeigen wir die Effektivität unseres Zugangs durch die Berechung der ionischen dielektrischen Funktion von Bariumtitanat und Strontiumtitanat bei Zimmertemperatur.

Acknowledgements

No part of this work could have been completed without the generous support of the Computational Materials Physics group at the Faculty of Physics of the University of Vienna. I deeply indebted to my supervisors, Georg Kresse and Menno Bokdam, who dedicated a great amount of their time to the completion of this thesis and whose guidance was essential for the success of this project.
Furthermore, I would like to thank Jonathan Lahnsteiner and Manuel Engel for being the most helpful and knowledgeable colleagues one could think of, Ferenc Karsai for helping me with the initialisation of thermally excited starting configurations for the MD simulations, and all other members of the group for the very supportive and motivating atmosphere.

Chapter 1

Introduction

A comprehensive model of the physical properties of a given material would be incomplete without a thorough understanding of the interaction of the material with external electromagnetic fields. In general, an external electromagnetic field will induce a displacement of the electric charge in the material, which in turn induces an electric dipole field. The strenght of the induced dipole depends on the polarisability of the material. To linear order, the polarisability can be described in terms of the frequency-dependent dielectric tensor $\epsilon(\omega)$.

The most important contributions to the dielectric function stem from electronic excitations and the ionic polarisability. While electronic exctitations have characteristic frequencies similar to visible light and above, peaks of the ionic polarisability are usually found at lower frequencies ranging up to infrared light. In this thesis, we are exclusively concerned with methods for the calculation of ionic contributions to the dielectric tensor of a material.

In modern density-functional theory (DFT) calculations, computing the ionic polarisability in the groundstate is a routine operation. However, in many cases, knowing the optical properties at 0 K is insufficient to make predictions about the dielectric function at higher temperatures. The discrepancy between the polarisability in the groundstate and at higher temperatures becomes most important if the material undergoes a phase transition as a result of increased temperature.

Furthermore, there is an important class of materials, of which perovskites are part, whose structures become what is known as 'dynamically stable' at temperatures around 300 K. If a system at non-zero temperature is dynamically stable, its equilibrium structure consists of not only one unique configuration, but of many different configurations of approximately the same energy. The system jumps back and forth between these configurations, and the macroscopic equilibrium structure can then be best described by an ensemble average of this set of ground-state structures. This property makes it virtually impossible to determine the dielectric properties from a single DFT calculation.

The purpose of this thesis is to go beyond the routine method of calulating dielectric properties in DFT and to present a statistical approach to the calculation of the polarisability at non-zero temperatures. This is achieved by means of a so-called Kubo-Green relation, which can be thought of as a generalisation of quantum perturbation theory to statistical mechanics. By deriving the appropriate Kubo-Green relation, we are able to describe the out-of-equilibrium response of a statistical system to an external perturbation in terms of its equilibrium fluctuations. These relations can be derived from a statistical-mechanical theorem known as the fluctuation-dissipation (FD) theorem.

The thesis is organised as follows: In chapter 2, we start by presenting the theoretical concepts needed to prepare the proof of the fluctuation-dissipation theorem. Next, we derive the

FD theorem following two different, and complementary approaches. Lastly, we also discuss the theoretical foundations of the standard method for computing dielectric properties at 0K, which is based on a calculation of the phonon spectrum of the crystal. We will refer to this method as 'phonon response'.

In chapter 3, we apply the methods of the previous chapter and derive expressions for the ionic polarisability of infinite crystals. From the FD theorem, we derive three equivalent formulae for the dielectric response, and show how they are related among themselves. Furthermore, we discuss the special case of the Kubo-Green relation for a delta-like perturbation, which will lead to a substantial reduction of the computational demands of the method. We refer to this simplification as 'delta-pulse' method. Lastly, we motivate the formula for calculating the phonon response of a crystal and show that it can be obtained as a limiting case of the Kubo-Green relation for the ionic polarisability.

Chapter 4 is dedicated to the implementation of the Kubo-Green relation for several example systems in the DFT simulation package VASP. The example systems, barium titanate and strontium titanate, have very interesting dielectric properties paired with pronounced structural instability both in the groundstate and at higher temperatures. We discuss the difficult relaxation process that lead to the inital configurations of the systems, and give computational details for the simulations.

Consequently, we present and discuss the results of the different approaches in chapter 5. We show the performance of Kubo-Green both at very low and higher temperatures, and compare its results to the phonon response at 0 K. Furthermore, we demonstrate the effectiveness of the delta-pulse method when applied to a fully-relaxed system.

Finally, in chapter 6, we provide a summary of all applied methods and results, and give an outlook for potential applications of the methods described in this thesis.

Chapter 2

Theory

The aim of this chapter is twofold: Firstly, we present the basic concepts needed to understand the FD theorem and show how to prove it. In fact, we will present two derivations of the theorem: one following the original, mathematically abstract paper by Ryogo Kubo (see ref. [1]), and the other after a paper by Robert Zwanzig (see [2]), which takes a more physical approach.
Secondly, we will give an overview of the theory that will lead us to the formulation of the phonon response in the next chapter. We discuss the dynamical matrix of an infinite crystal, phonon modes and eigenfrequencies, and introduce the concept of Born effective charges.

2.1 Basic concepts

2.1.1 Time-independent perturbation theory

There is definitely no lack of excellent textbooks on perturbation theory, which is why we only give a brief overview of the topic and to derive the most important equations. For further details we refer to the book by J.J. Sakurai (see reference [3]).

We consider a quantum system in an d-dimensional Hilbert space ($d \leq \infty$), described by the Hamiltonian H^0. Assume that we know all its (normalised) eigenvectors $|\Psi_n^0\rangle$ and the corresponding eigenenergies E_n^0 as solutions of the Schrödinger equation

$$H^0|\Psi_n^0\rangle = E_n^0|\Psi_n^0\rangle. \tag{2.1}$$

From this, we want to construct solutions for a slightly different ('perturbed') system

$$H = H^0 + \lambda H^1, \tag{2.2}$$

where H^0 is our original Hamiltonian, and the effect of λH^1 is small compared H^0. In other words, we want to solve the eigenvalue equation

$$H|\Psi_n\rangle = E_n|\Psi_n\rangle. \tag{2.3}$$

The main idea of perturbation theory is to expand the eigenstates $|\Psi_n\rangle$ and eigenenergies E_n of the full Hamiltonian H in powers of the perturbation. We use a factor λ to help us organise terms of similar order of the expansion. At the end of this section, λ will be set to 1. We have

$$E_n = E_n^0 + \lambda E_n^1 + \lambda^2 E_n^2 + ... \tag{2.4}$$

$$|\Psi_n\rangle = |\Psi_n^0\rangle + \lambda|\Psi_n^1\rangle + \lambda^2|\Psi_n^2\rangle + ... \tag{2.5}$$

The only requirement for the series is that in the limit of vanishing perturbation, we recover the unperturbed eigenstates and eigenenergies, that is,

$$\lim_{\lambda\to 0}|\Psi_n\rangle = |\Psi_n^0\rangle \qquad \text{and} \qquad \lim_{\lambda\to 0} E_n = E_n^0.$$

In most cases, one is only interested in first-order corrections to the initial states and energies, which is why we will always truncate the expansion after the linear term.

For practical purposes, we want the new eigenstates $\{|\Psi_n\rangle\}$ to be normalised to one,

$$\langle\Psi_n|\Psi_n\rangle = 1 \qquad \forall n. \tag{2.6}$$

Furthermore, we require that the unperturbed eigenstates $|\Psi_n^0\rangle$ are also normalised. This implies

$$1 = \langle\Psi_n|\Psi_n\rangle = \underbrace{\langle\Psi_n^0|\Psi_n^0\rangle}_{=1} + \lambda\langle\Psi_n^0|\Psi_n^1\rangle + \lambda\langle\Psi_n^1|\Psi_n^0\rangle + O(\lambda^2),$$

and in particular,

$$\langle\Psi_n^0|\Psi_n^1\rangle = 0, \tag{2.7}$$

as $\lambda \neq 0$. We rewrite (2.3) using the series expansions,

$$\begin{aligned} H|\Psi_n\rangle &= \big(H^0 + \lambda H^1\big)\big(|\Psi_n^0\rangle + \lambda|\Psi_n^1\rangle + ...\big) \\ &= \big(E_n^0 + \lambda E_n^1 + ...\big)\big(|\Psi_n^0\rangle + \lambda|\Psi_n^1\rangle + ...\big) = E_n|\Psi_n\rangle, \end{aligned}$$

and for the first-order correction we obtain

$$\lambda H^0|\Psi_n^1\rangle + \lambda H^1|\Psi_n^0\rangle = \lambda E_n^0|\Psi_n^1\rangle + \lambda E_n^1|\Psi_n^0\rangle. \tag{2.8}$$

Multiplying another base ket $\langle\Psi_n^0|$ from the left, and using equation (2.7), leads to

$$\begin{aligned} \langle\Psi_n^0|H^0|\Psi_n^1\rangle + \langle\Psi_n^0|H^1|\Psi_n^0\rangle &= E_n^0\langle\Psi_n^0|\Psi_n^1\rangle + E_n^1\langle\Psi_n^0|\Psi_n^0\rangle \\ = E_n^0\cancel{\langle\Psi_n^0|\Psi_n^1\rangle} + \langle\Psi_n^0|H^1|\Psi_n^0\rangle &= E_n^0\cancel{\langle\Psi_n^0|\Psi_n^1\rangle} + E_n^1, \end{aligned}$$

and the first-order energy correction becomes

$$E_n^1 = \langle\Psi_n^0|H^1|\Psi_n^0\rangle. \tag{2.9}$$

The eigenenergies of the full Hamiltonian H is therefore given by

$$E_n = E_n^0 + \lambda\langle\Psi_n^0|H^1|\Psi_n^0\rangle. \tag{2.10}$$

We can also derive an expression to compute the first-order correction $|\Psi_n^1\rangle$ to the eigenstates of H. To this end, note that it must be possible to expand $|\Psi_n^1\rangle$ in the basis of unperturbed eigenstates $\{|\Psi_n^0\rangle\}_{n=0}^{\infty}$, because they span the whole Hilbert space. Consequently, we write

$$|\Psi_n^1\rangle = \sum_{m\neq n} c_m|\Psi_m^0\rangle \qquad c_m = \langle\Psi_m^0|\Psi_n^1\rangle$$

Multiplication of (2.8) from the left by any base ket $|\Psi_m^0\rangle \neq |\Psi_n^0\rangle$ yields

$$\begin{aligned} \langle\Psi_m^0|H^0|\Psi_n^1\rangle + \langle\Psi_m^0|H^1|\Psi_n^0\rangle &= E_n^0\underbrace{\langle\Psi_m^0|\Psi_n^1\rangle}_{c_m} + E_n^1\underbrace{\langle\Psi_m^0|\Psi_n^0\rangle}_{0} \\ \implies E_m^0 c_m + \langle\Psi_m^0|H^1|\Psi_n^0\rangle &= E_n^0 c_m \end{aligned}$$

The expansion coefficients c_m are given by

$$c_m = \frac{\langle\Psi_m^0|H^1|\Psi_n^0\rangle}{E_n^0 - E_m^0}.$$

We can thus write the first-order state correction $|\Psi_n^1\rangle$ as

$$|\Psi_n^1\rangle = \sum_{m\neq n} \frac{\langle\Psi_m^0|H^1|\Psi_n^0\rangle}{E_n^0 - E_m^0}|\Psi_m^0\rangle. \tag{2.11}$$

The eigenstate of the Hamiltonian $H = H^0 + \lambda H^1$ in first-order perturbation theory is

$$|\Psi_n\rangle = |\Psi_n^0\rangle + \lambda\sum_{m\neq n} \frac{\langle\Psi_m^0|H^1|\Psi_n^0\rangle}{E_n^0 - E_m^0}|\Psi_m^0\rangle. \tag{2.12}$$

2.1.2 Time-dependent perturbation theory

In this subsection, we generalise the idea introduced above to explicitly time-dependent perturbations $H^1(t)$. Since in quantum mechanics, there are two standard ways to describe the time-dependence of physical observables, namely the Schrödinger picture and the Heisenberg picture, we will present the main results of time-dependent perturbation theory in both pictures.

Recall that in the **Schrödinger** picture, states (state vectors) $|\Psi\rangle_S$ are time-dependent while observables (operators) A_S are independent of time, i.e.

$$|\Psi\rangle_S = |\Psi(t)\rangle_S \qquad \text{and} \qquad A_S(t) = A_S(0).$$

Wherever it is not obvious, we use the subscript S to indicate that a state or operator is given in the Schrödinger picture. Time evolution of the eigenstate $|\Psi_n\rangle$ is determined by the time-dependent Schrödinger equation

$$i\frac{\partial|\Psi_n(t)\rangle}{\partial t} = H|\Psi_n(t)\rangle, \tag{2.13}$$

whose solution is simply

$$|\Psi_n(t)\rangle = e^{-iHt}|\Psi_n(t=0)\rangle. \tag{2.14}$$

As before, we now consider a perturbed system

$$H = H^0 + H^1(t),$$

where the perturbation $H^1(t)$ is small compared to H^0 (cf. 2.2). Note that we set $\lambda = 1$ for the rest of this text. We simply insert this new Hamiltonian into equation (2.13),

$$i\frac{\partial|\Psi_n(t)\rangle}{\partial t} = \big[H^0 + H^1(t)\big]|\Psi_n(t)\rangle, \tag{2.15}$$

and impose the initial condition

$$|\Psi_n(t=0)\rangle = |\Psi_n^0\rangle,$$

where $|\Psi_n^0\rangle$ is the n-th eigenvalue of the unperturbed Hamiltonian H^0. In analogy to (2.4) and (2.5), we expand $|\Psi_n(t)\rangle$ into a series

$$|\Psi_n(t)\rangle = |\Psi_n^0(t)\rangle + |\Psi_n^1(t)\rangle + ...$$

Insert the series expansion into (2.15), and seperate the constant and linear contributions. We have

$$i\frac{\partial|\Psi_n^0(t)\rangle}{\partial t} = H^0|\Psi_n^0(t)\rangle, \qquad \text{with the solution} \qquad |\Psi_n^0(t)\rangle = e^{-iH^0t}|\Psi_n^0\rangle, \tag{2.16}$$

and

$$i\frac{\partial|\Psi_n^1(t)\rangle}{\partial t} = H^0|\Psi_n^1(t)\rangle + H^1(t)|\Psi_n^0(t)\rangle. \tag{2.17}$$

Integrating (2.17) gives

$$|\Psi_n^1(t)\rangle = -ie^{-iH^0t}\int_0^t e^{iH^0t'}H^1(t')|\Psi_n^0(t')\rangle dt' + e^{-iH^0t}|\Psi_n^1(t=0)\rangle. \tag{2.18}$$

We can check this by computing the time-derivative of (2.18). As we have to differentiate with respect to the integration limit, we must respect Leibnitz' integral rule.

Using the Leibnitz rule, we obtain

$$i\frac{\partial|\Psi_n^1(t)\rangle}{\partial t} = H^0\Big[(-i)e^{-iH^0t}\int_0^t e^{iH^0t'}H^1(t')|\Psi_n^0(t')\rangle dt'\Big] + H^1(t)|\Psi_n^0(t)\rangle + H^0e^{-iH^0t}|\Psi_n^1(0)\rangle$$

$$= H^0|\Psi_n^1(t)\rangle + H^1(t)|\Psi_n^0(t)\rangle + H^0|\Psi_n^1(0)\rangle.$$

For simplicity, we can say that the perturbation vanishes before $t = 0$, which implies $|\Psi^1(t = 0)\rangle = 0$. The final solution for (2.15) then becomes

$$|\Psi_n(t)\rangle = e^{-iH^0t}|\Psi_n^0\rangle - i\int_0^t e^{-iH^0(t-t')}H^1(t')|\Psi_n^0(t')\rangle dt'$$

$$= e^{-iH^0t}|\Psi_n^0\rangle - i\int_0^t e^{-iH^0(t-t')}H^1(t')e^{-iH^0t'}|\Psi_n^0\rangle dt'. \quad (2.19)$$

Next, we turn to the **Heisenberg** picture. To ensure consistency with results from the Schrödinger picture, we require that expectation values of the form

$$\langle A\rangle_t = \langle\Psi(t)|A_S|\Psi(t)\rangle_S \quad (2.20)$$

remain invariant under a transformation between pictures. This makes sense, as the expectation value corresponds to actual physical measurements, which must of course be independent of the picture we choose to describe it. We can rewrite this expectation value as

$$\langle O\rangle_t = \langle\Psi(0)|\underbrace{e^{iHt}A_S\,e^{-iHt}}_{:=A_H(t)}|\Psi(0)\rangle_S. \quad (2.21)$$

Note that the index S added to a product $\langle\Psi|A|\Psi\rangle_S$ means that both the bra $\langle\Psi|$ and the ket $|\Psi\rangle$ belong to the Schrödinger picture. Following (2.21), operators in the Heisenberg and Schrödinger pictures are related to one another through

$$A_H(t) = e^{iHt}A_S\,e^{-iHt} \qquad \Longleftrightarrow \qquad A_S(t) = e^{-iHt}A_H\,e^{iHt}. \quad (2.22)$$

Consequently, states must follow the transformation

$$|\Psi\rangle_H = e^{iHt}|\Psi(t)\rangle_S \qquad \Longleftrightarrow \qquad |\Psi(t)\rangle_S = e^{-iHt}|\Psi\rangle_H \quad (2.23)$$

With this definition for the Heisenberg representation of the observable $A_H(t)$, time-dependence follows the time-evolution of the operators, and not of the states. The Heisenberg equation of motion is given by

$$i\frac{\partial A_H(t)}{\partial t} = -He^{iHt}A_S\,e^{-iHt} + e^{iHt}A_SHe^{-iHt} = \big[A_H, H\big]. \quad (2.24)$$

To describe the linear response to an external perturbation in the Hamiltonian, we now have to expand the operator $A(t)$ into a series,

$$A = A^0(t) + A^1(t) + ...,$$

and insert the expanded operator and the perturbed Hamiltonian into the Heisenberg equation

$$i\frac{\partial}{\partial t}\big[A^0(t) + A^1(t)\big] = \big[A^0(t) + A^1(t), H^0 + H^1(t)\big]. \quad (2.25)$$

Separation of the constant and first-order terms leads to

$$i\frac{\partial A^0(t)}{\partial t} = \big[A^0(t), H^0\big] \qquad \text{with} \qquad A^0(t) = e^{iH^0}A^0(0)e^{-iH^0t}, \quad (2.26)$$

and

$$i\frac{\partial A^1(t)}{\partial t} = \big[A^0(t), H^1(t)\big] + \big[A^1(t), H^0\big]. \tag{2.27}$$

The solution to (2.27) is analogous to (2.18), and is given by

$$A^1(t) = -i\int_0^t e^{iH^0(t-t')}\big[A^0(t), H^1(t')\big]e^{-iH^0(t-t')}dt'. \tag{2.28}$$

This can be verified by differentiation; mind again Leibnitz' integral rule

$$\begin{aligned} &i\frac{\partial A^1(t)}{\partial t} = \big[A^0(t), H^1(t)\big] \\ &-H^0\left[i\int_0^t e^{iH^0(t-t')}\big[A^0(t), H^1(t')\big]e^{-iH^0(t-t')}dt'\right] + \left[i\int_0^t e^{-iH^0(t-t')}\big[A^0(t), H^1(t')\big]e^{-iH^0(t-t')}\right]H^0 \\ &\qquad = \big[A^0(t), H^1(t)\big] + \big[A^1(t), H^0\big]. \end{aligned}$$

Expressions (2.19) and (2.28) are two equivalent descriptions of the first-order response of a quantum system to a time-dependent perturbation, and it is very easy to transform one into the other using (2.22) and (2.23).

In the following section, we will present a third picture to describe time evolution and time-dependent perturbation.

2.1.3 Time-dependent perturbation in the interaction picture

Clearly, the choice of picture to describe the dynamics of a system is arbitrary, as long as the expectation value (2.20) remains invariant. This means that we have some freedom to select a description of time-dependence in which equations of time-dependent perturbation theory take a simple form.

Such a picture exists, it is called the interaction picture (IP), and we will present it in this section. In the derivation of the FD theorem, we will make repeated use of the interaction picture representation. As before, states and operators will bear a subscript S, H or I, indicating the Schrödinger, Heisenberg and interaction picture, respectively.

In the previous section, we saw that computing the time dependence of a state (or observable) can become somewhat involved if the full Hamiltonian is of the form

$$H = H^0 + H^1(t).$$

Both parts of the full Hamiltonian H contribute to time evolution. The unperturbed H^0 gives rise to what is sometimes called the 'natural' motion of the system, while the time-dependent $H^1(t)$ causes small deviations from that natural motion. One finds that the equations of motion in time-dependent perturbation theory can be simplified if time-dependence on H^0 and $H^1(t)$ is shared among states and operators.

In the Schrödinger picture, time evolution follows the equation

$$|\Psi_n(t)\rangle = e^{-iHt}|\Psi_n(t=0)\rangle, \tag{2.14}$$

whose solution can be expressed by means of the time-evolution operator

$$T_S(t-t_0) = e^{-iH(t-t_0)},$$

so that the states evolve according to

$$|\Psi(t)\rangle_S = T_S(t)|\Psi(t=0)\rangle_S.$$

Taking the derivative of $T_S(t)$ with respect to time, we recover a Schrödinger-type equation for the time-evolution operator (cf. 2.13),

$$i\frac{\partial T_S}{\partial t} = HT_S(t). \tag{2.29}$$

For a perturbed Hamiltonian, the full time evolution in the Schrödinger picture,

$$T_S(t) = e^{-i(H^0+H^1(t))t}$$

can be split up into the two parts,

$$T^0 = e^{-iH^0t} \quad \text{and} \quad T_I(t) = e^{-iH^1(t)t}.$$

The idea of the interaction picture is to transfer the time-dependence caused by H^0 away from the state vector to the operator. This is achieved by the transformation

$$|\Psi(t)\rangle_I = e^{iH^0t}|\Psi(t)\rangle_S \qquad \Longleftrightarrow \qquad |\Psi(t)\rangle_S = e^{-iH^0t}|\Psi(t)\rangle_I. \tag{2.30}$$

This means that in order to conserve the expectation value, the time-dependence of $|\Psi(t)\rangle_I$ on H^0 must be accounted for in the time evolution of the operator. Thus, the operators in the interaction picture are linked to the Schrödinger picture according to

$$A_I = e^{iH^0t}A_S\, e^{-iH^0t} \qquad \Longleftrightarrow \qquad A_S = e^{-iH^0t}A_I\, e^{iH^0t}. \tag{2.31}$$

A similar relation between the interaction and the Heisenberg picture can be shown easily. In this case, one has to transfer the time dependence on $H^1(t)$ from the operator to the state vector. The state is then given by

$$|\Psi(t)\rangle_I = e^{-iH^1(t)t}|\Psi(0)\rangle_H \qquad \Longleftrightarrow \qquad |\Psi(t)\rangle_H = e^{iH^1(t)t}|\Psi(0)\rangle_I, \tag{2.32}$$

and the operator by

$$A_I = e^{iH^1(t)t}A_H\, e^{-iH^1(t)t} \qquad \Longleftrightarrow \qquad A_H = e^{-iH^1(t)t}A_I\, e^{iH^1(t)t}. \tag{2.33}$$

To see that this change of picture can indeed simplify our equations of motion, we now derive the Schrödinger equation in the interaction picture. Starting from (2.13), we write

$$i\frac{\partial}{\partial t}\left[e^{-iH^0t}|\Psi(t)\rangle_I\right] = \left[H_S^0 + H_S^1(t)\right]e^{-iH^0t}|\Psi(t)\rangle_I$$

$$\Longleftrightarrow \cancel{H^0e^{-iH^0t}|\Psi(t)\rangle_I} + ie^{-iH^0t}\frac{\partial|\Psi(t)\rangle_I}{\partial t} = \cancel{H^0e^{-iH^0t}|\Psi(t)\rangle_I} + H^1(t)e^{-iH^0t}|\Psi(t)\rangle_I$$

$$\Longleftrightarrow i\frac{\partial\Psi(t)\rangle_I}{\partial t} = e^{iH^0t}H_S^1(t)e^{-iH^0t}|\Psi(t)\rangle_I = H_I^1(t)|\Psi(t)\rangle_I \tag{2.34}$$

In the last step, we recovered the perturbation Hamiltonian in the interaction picture (cf. 2.31),

$$H_I^1(t) = e^{iH^0t}H_S^1(t)e^{-iH^0t}.$$

Equation (2.34) is the interaction equation of motion for the system and is equivalent to the Schrödinger (2.15) and Heisenberg (2.25) equations of motion.

We will now look for a solution for the interaction equation of motion. Via

$$i\frac{\partial|\Psi(t)\rangle_I}{\partial t} = H_I^1|\Psi(t)\rangle_I = i\frac{\partial T_I(t)}{\partial t}|\Psi(0)\rangle = H_I^1 T_I(t)|\Psi(0)\rangle,$$

we obtain a differential equation for the partial time-evolution operator $T_I(t)$ which is very similar to equation (2.29),

$$i\frac{\partial T_I(t)}{\partial t} = H_I^1 T_I(t), \quad \text{with} \quad T_I(t) = e^{-iH^1(t)t}$$

Integration yields

$$T_I(t,t_0) = \mathbb{1} - i\int_{t_0}^{t} H_I^1(t')T_I(t',t_0)dt'. \tag{2.35}$$

With $T_I(t)$ appearing on either side of the equation, the last step does not seem like a step forward. However, it is very easy to determine constant and linear contributions to (2.35). All terms proportional to $\left(H_I^1(t)\right)^2$ appearing in the expansion for $T_I(t)$ are of second order and can be omitted. Consequently, we move ahead by setting

$$T_I(t_0,t') = e^{iH_I^1(t'-t_0)} \approx \mathbb{1}$$

on the right-hand side of (2.35). We obtain

$$T_I(t,t_0) = \mathbb{1} - i\int_{t_0}^{t} H_I^1(t')dt' + O(H_I). \tag{2.36}$$

With this result for the partial time-evolution operator $T_I(t)$, we can solve the equation of motion in the interaction picture

$$|\Psi(t)\rangle_I = T_I(t)|\Psi(0)\rangle_I = |\Psi(0)\rangle_I - i\int_0^t H_I^1(t')|\Psi(0)\rangle_I dt'.$$

Remember that due to the initial conditions,

$$|\Psi(t=0)\rangle_I = |\Psi(t=0)\rangle_S = |\Psi_n^0\rangle$$

we have

$$|\Psi_n(t)\rangle_I = |\Psi_n^0\rangle - i\int_0^t H_I^1(t')|\Psi_n^0\rangle_I dt'. \tag{2.37}$$

Compare equation (2.37) to the equivalent solution in the Schrödinger picture (2.19). The formal simplification is obvious. Furthermore, it is straightforward to transform equation (2.37) back to the Schrödinger picture using (2.30) and (2.31):

$$|\Psi(t)\rangle_S = e^{-iH^0t}|\Psi^0(0)\rangle_S - i\int_0^t e^{-iH^0(t-t')}H_S^1(t')e^{-iH^0t'}|\Psi^0(0)\rangle_S dt',$$

which is exactly the same as (2.19).

Example application: Fermi's Golden Rule

To conclude this section, we consider a simple example system to which we apply a time-dependent perturbation $H^1(t)$ to H^0. With this example, we can show a more general principle known as Fermi's Golden Rule.

Consider a Hamiltonian $H = H^0 + H^1(t)$ where the time-dependent perturbation is explicitly given by

$$H^1(t) = Ve^{i\omega t+\eta t}.$$

Here, V is a constant, and the factor $e^{\eta t}$ $(0 < \eta \ll 1)$ simulates a slow turning-on of the perturbation as t goes from $-\infty$ to 0. Also, note that in the limit $\omega = 0$ we recover the special case of constant perturbation.

At the infinite past, i.e. at $t = -\infty$, the Hamiltonian is in its ground state, i.e. $H = H^0$. Let $|\Psi_n^0\rangle$ be an eigenstate of H^0 with energy E_n^0. In the interaction picture, its time evolution must follow

$$|\Psi_n(t)\rangle = T_I(t)|\Psi_n^0\rangle \qquad \text{with } T_I(t) = \mathbb{1} - i\int_{t_0}^{t} H_I^1(t')dt' + O(H_I)$$

At a later time $t > -\infty$, there is a non-zero overlap between the state $|\Psi_n(t)\rangle$ and another eigenstate of H^0, $|\Psi_m^0\rangle$, given by

$$\langle\Psi_m^0|\Psi_n(t)\rangle = \langle\Psi_m^0|T_I(t)|\Psi_n^0\rangle = \langle\Psi_m^0|\Psi_n^0\rangle - i\int_0^t dt'\langle\Psi_m^0|H_I^1(t')|\Psi_n\rangle + ...$$

Since we know $H_I^1(t)$ explicitly, we can evaluate the bracket in the integral,

$$\langle\Psi_m^0|H_I^1(t')|\Psi_n^0\rangle = \langle\Psi_m^0|e^{iH^0t}V\,e^{-iH^0t}|\Psi_n^0\rangle e^{i\omega t+\frac{\eta}{2}t} = e^{-i(E_n^0-E_m^0)t'}\langle\Psi_m^0|V|\Psi_n^0\rangle e^{i\omega t+\eta t}.$$

To simplify notation, we define

$$\omega_{mn} := E_n^0 - E_m^0 \qquad \text{and} \qquad V_{mn} := \langle\Psi_m^0|V|\Psi_n^0\rangle.$$

A non-zero overlap between states leads to a non-zero transition probability, which is simply the absolute square of the transition amplitude,

$$p_{n\to m}(t) = \left|\langle\Psi_m^0|T_I(t)|\Psi_n^0\rangle\right|^2 = \left|\int_{-\infty}^{t} V_{mn}e^{i(\omega-\omega_{mn}-i\eta)t'}dt'\right|^2$$
$$= |V_{mn}|^2\left|\frac{e^{i(\omega-\omega_{mn}-i\eta)t}}{\omega-\omega_{mn}-i\eta}\right|^2 = |V_{mn}|^2\frac{e^{2\eta t}}{(\omega_{mn}-\omega)^2+\eta^2}.$$

At $t = 0$, the first-order transition probability $p_{n\to m}$ is given by

$$p_{n\to m}(t=0)\lim_{\eta\to 0} = \frac{|V_{mn}|^2}{(\omega_{mn}-\omega)^2+\eta^2}. \tag{2.38}$$

Furthermore, we can use the identity

$$\lim_{\eta\to 0}\frac{\eta}{(x-x_0)^2+\eta^2} = \pi\delta(x-x_0)$$

to compute the rate

$$\frac{dp_{n\to m}}{dt} = \lim_{\eta\to 0}\ |V_{mn}|^2\frac{2\eta}{(\omega-\omega_{mn})^2+\eta^2}\,e^{2\eta t} = 2\pi|V_{mn}|^2\delta(\omega_{mn}-\omega). \tag{2.39}$$

Equation (2.81) is known as **Fermi's Golden Rule** and describes the rate of the transitions caused by an external potential. It describes the probability per unit time for a particle to be excited from an initial state $|\Psi_n^0\rangle$ to an excited state $|\Psi_m^0\rangle$.

2.1.4 Density matrix and phase-space integration in classical and quantum mechanics

Before we move on to the actual derivation of Kubo-Green, we introduce the concept of phase space integration in classical and quantum mechanics and discuss some properties of the density matrix.

As we will see in the next section, the fluctuation-dissipation theorem is only valid for statistical ensembles. It relates the fluctuations of an obervable around its equilibrium value to the response to an external perturbation. In most cases, we do not have direct access to the total energy of the system, but we can control its temperature. Such systems are then best described in a canonical ensemble. In this section, we introduce the density matrix of a canonical ensemble and show some of the properties which will be useful later on.

First, consider some quantity $A = A(q, p)$ defined on a classical, $6N$-dimensional phase space Γ, where N is the number of particles, q denotes the $3N$ position coordinates and p denotes the $3N$ momenta. To obtain the phase-space average of A, we have to evaluate the phase-space integral

$$\langle A \rangle = \int d\,\Gamma A(q,p) f(q,p). \tag{2.40}$$

In (2.40), $f(q, p)$ is the density of states in Γ. In a canonical ensemble at temperature T, this density of states is given by

$$f(q,p) = \frac{1}{Q}\, e^{-\beta E(q,p)}, \tag{2.41}$$

where the factor $\beta = (k_B T)^{-1}$ is the inverse temperature, k_B is Boltzmann's constant, the total energy associated to the state (q, p) is $E(q, p)$, and Q is the canonical partition function

$$Q = \int d\,\Gamma e^{-\beta E(q,p)}.$$

In equilibrium, the density of states $f(q, p)$ is by definition time-independent.

If we want to derive an expression similar to (2.40) for a quantum system, we must introduce the concept of the density matrix of a state. We call

$$\rho = |\Psi\rangle\langle\Psi|$$

the density operator of the 'pure' state $|\Psi\rangle$. The pure state is described by a wavefunction, but does not necessarily have to be an energy eigenstate. More generally, we can also define a density operator for a mixed state

$$|\Psi\rangle = \sum_i p_i |\Psi_i\rangle$$

as

$$\rho := \sum_i p_i |\Psi_i\rangle\langle\Psi_i|. \tag{2.42}$$

The mixed state is a statistical superposition of pure states, where each individual state is measured with a (real) probability p_i. The $|\Psi_i\rangle$ are normalised, and we will assume that they are orthogonal to one another. Also the operator ρ must fulfil a normalisation condition, given by

$$\mathrm{Tr}(\rho) = 1$$

The trace of the operator A is defined as

$$\mathrm{Tr}\ (A) = \sum_n \langle\phi_n|A|\phi_n\rangle,$$

where the states $|\phi_n\rangle$ form an orthonormal basis of the Hilbert space. Note that the trace has the cyclic property

$$\mathsf{Tr}\big(ABC\big) = \mathsf{Tr}\big(BCA\big) = \mathsf{Tr}\big(CAB\big). \tag{2.43}$$

Imposing normalisation to (2.42) implies

$$\mathsf{Tr}\ \big(\rho\big) = \mathsf{Tr}\Big[\sum_i p_i|\Psi_i\rangle\langle\Psi_i|\Big] = \mathsf{Tr}\ \Big[\sum_i p_i\langle\Psi_i|\Psi_i\rangle\Big] = \sum_i p_i = 1.$$

To see why ρ has the property of a density, note that the expectation value of an observable A with respect to the mixed state $|\Psi\rangle$ can be conveniently expressed as

$$\mathsf{Tr}\big(\rho A\big) = \mathsf{Tr}\Big[\sum_i p_i|\Psi_i\rangle\langle\Psi_i|A\Big] = \sum_i p_i\langle\Psi_i|A|\Psi_i\rangle = \langle A\rangle. \tag{2.44}$$

In analogy to (2.41), we write the density matrix of a system in a canononical ensemble at inverse temperature β as

$$\rho_\beta = \frac{e^{-\beta H}}{\mathsf{Tr}\ e^{-\beta H}} = \frac{e^{-\beta E_n}}{\sum_n e^{-\beta E_n}},$$

where the second equation is only strictly true in the basis which diagonalises the Hamiltonian H. The quantum partition function Q for the canonical ensemble is obviously $Q = \mathsf{Tr}\ e^{-\beta H}$.

Like the density of states $f(q,p)$ in the classical case, ρ_β describes the density of states in equilibrium, i.e. ρ_β is independent of time. This can be seen easily if we insert ρ_β in the Heisenberg equation of motion,

$$i\frac{\partial\rho_\beta}{\partial t} = \big[\rho_\beta, H\big] = \frac{1}{\mathsf{Tr}\ e^{-\beta H}}\big[e^{-\beta H}, H\big] = 0. \tag{2.45}$$

To see why last equality in (2.45) holds we just have to remind ourselves that the matrix exponential e^H is defined via the infinite series

$$e^H = \sum_{n=0}^{\infty}\frac{(H)^n}{n!},$$

and that

$$\big[H^n, H\big] = 0.$$

Finally, we introduce a very special property of the canonical density matrix. This property, known as Kubo transform, will play a central part in the derivation of the FD theorem, compare equation (3.7) in ref. [1].

$$\begin{aligned}\big[A, e^{-\beta H}\big] &= e^{-\beta H}\int_0^\beta e^{H\tau}\big[H, A\big]e^{-H\tau}d\tau = -ie^{-\beta H}\int_0^\beta e^{H\tau}\dot{A}e^{-H\tau}d\tau \\ &= -\,ie^{-\beta H}\int_0^\beta \dot{A}(-i\tau)d\tau.\end{aligned} \tag{2.46}$$

According to (2.46), the commutator of some operator A with $e^{-\beta H}$ can be written as an integral over the time-derivative of A evaluated between 0 and the inverse temperature along the axis of imaginary time $i\tau$. To calculate $\dot{A}(-i\tau)$, one first has to take the ordinary time-derivative of A along the real axis, extend its domain to the imaginary axis, and evaluate it at $i\tau$.

To prove the Kubo transform (2.46), we proceed in the opposite direction:

$$\begin{aligned}e^{-\beta H}\int_0^\beta \dot{A}(-i\tau)d\tau &= e^{-\beta H}\int_0^\beta \big[e^{\tau H}A\,e^{-\tau H}, H\big]d\tau = e^{-\beta H}\int_0^\beta d\tau\frac{d}{d\tau}\Big(e^{\tau H}A\,e^{-\tau H}\Big) \\ &= e^{-\beta H}\Big[e^{\tau H}A\,e^{-\tau H}\Big]_{\tau=0}^{\beta} = A\,e^{-\beta H} - e^{-\beta H}A = \big[A, e^{-\beta H}\big]\end{aligned}$$

2.2 Derivation of the Kubo-Green relation

Having covered the basic concepts in section (2.1), we can now move on to the proof of the fluctuation-dissipation (FD) theorem. With the result of the FD theorem (equation 2.64), we will derive a Kubo-Green relation that will allow us to compute the frequency-dependent ionic polarisability $\chi(\omega)$ of an infinite crystal at non-zero temperature.

The FD theorem shows that, in the same way that we can describe the first-order response of a simple quantum-mechanical system to some external perturbation in terms of its equilibrium eigenstates, we can also express the linear out-of equilibrium response of a large statistical-mechanical system by means of some equilibrium property.

In the framework of the FD theorem, the linear response of an observable in a large system to a perturbation is described as a time-correlation function of the fluctuations of that observable around its equilibrium value. The exact type of correlation function required depends on the type of perturbation that we want to describe. As we will see in the next chapter, the ionic polarisability $\epsilon(\omega)$ can be obtained from the equilibrium fluctuations of the total dipole moment of the system.

2.2.1 Kubo's proof of the fluctuation-dissipation theorem

Although it may be inaccurate to attribute the idea of the FD theorem to Ryogo Kubo alone[1], it remains true that his paper on the 'Statistical-Mechanical Theory of Irreversible Processes I' (ref. [1]) is regarded as the standard reference in this field. In the following, we give a detailed account of his results.

We consider a quantum-mechanical system H^0 in equilibrium which experiences a time-dependent perturbation $H^1(t)$. Initially, that is at time $t < 0$, the perturbation vanishes, and the system in equilibrium is described by some density matrix

$$\rho^0 = \sum_i p_i |\Psi_i^0\rangle\langle\Psi_i^0|,$$

satisfying the equilibrium condition (2.45)

$$i\frac{\partial \rho^0}{\partial t} = \left[\rho^0, H^0\right] = 0.$$

At time $t = 0$, we turn on a small perturbation $H^1(t)$. With this, we get a new total density $\rho(t)$, which we can expand, as before, in a series

$$\rho(t) = \rho^0 + \rho^1(t) + ...$$

The full density operator evolves over time according to the Heisenberg equation (2.25),

$$i\frac{\partial \rho(t)}{\partial t} = \left[\rho^0 + \rho^1(t), H^0 + H^1(t)\right],$$

whose solution, according to (2.26) and (2.28), is

$$\rho(t) = \rho^0 - i\int_0^t e^{iH^0(t-t')}\left[\rho^0, H^1(t')\right]e^{-iH^0(t-t')}dt' \tag{2.47}$$

[1] Compare e.g. the introductory remarks of chapter 2 in Zwanzig's paper [2]

As in (2.44), we use our density matrix (2.47) to express the expectation value of some quantity B defined in the Hilbert space. As the density matrix $\rho = \rho(t)$ now dependends on time explicitly, also the expectation value $\langle B(t)\rangle$ becomes time-dependent:

$$\langle B(t)\rangle = \mathsf{Tr}\big[\rho(t)B\big]. \tag{2.48}$$

We can seperate the constant and linear terms of $B(t) = B^0 + B^1(t)$ as

$$\langle B^0\rangle = \mathsf{Tr}\big[\rho^0 B\big]$$

and

$$\langle B^1(t)\rangle = \mathsf{Tr}\big[\rho^1(t)B\big] = -i\,\mathsf{Tr}\bigg[\int_0^t e^{iH^0(t-t')}\big[\rho^0, H^1(t')\,\big]e^{-iH^0(t-t')}B(t')\,dt'\bigg]. \tag{2.49}$$

Comparison with (2.31) shows that

$$e^{iH^0(t-t')}\big[\rho^0, H^1(t')\,\big]_S\, e^{-iH^0(t-t')} = \big[\rho^0, H^1(t-t')\big]_I$$

is just the representation of the commutator in the interaction picture, and we can rewrite (2.49) as

$$\langle B^1(t)\rangle = -i\,\mathsf{Tr}\bigg[\int_0^t \big[\rho^0, H^1(t-t')\,\big]B(t')\,dt'\bigg].$$

After a shift of the integration variable $t' \to t - t'$, we recover the relation

$$\langle B^1(t)\rangle = -i\int_0^t \mathsf{Tr}\Big[\big[\rho^0, H^1(t')\,\big]B(t-t')\Big]\,dt', \tag{2.50}$$

where all operators are to be taken in the interaction picture. Equation (2.50) is the central result of the FD theorem. In close analogy to our result in section 2.1, we were able to express the first-order response $B^1(t)$ in terms of the equilibrium flucutations $B^0(t)$.

To simplify notation, we want to write the change of $\langle B(t)\rangle$ as an integral over time of a response function $\phi(t)$, i.e.,

$$\langle B^1(t)\rangle = \int_0^t \phi(t-t')dt'. \tag{2.51}$$

Comparison with (2.50) gives us

$$\phi(t-t') = -i\,\mathsf{Tr}\Big[\big[\rho^0, H^1(t')\big]\,B(t-t')\Big]. \tag{2.52}$$

Observing the cyclic property of the trace,

$$\mathsf{Tr}\big(ABC\big) = \mathsf{Tr}\big(BCA\big) = \mathsf{Tr}\big(CAB\big), \tag{2.43}$$

we arrive at

$$\phi(t-t') = i\,\mathsf{Tr}\Big[\rho^0\big[H^1(t'), B(t-t')\big]\Big]. \tag{2.53}$$

Finally, we want that the response function $\phi(t)$ decays to zero for very large times, i.e. that

$$\lim_{t\to\infty}\phi(t) = 0.$$

However, if the Fourier transform of $\phi(t)$ has a non-zero value at $\omega = 0$, the response will instead converge towards a finite constant. Therefore, we redefine $\phi(t)$ according to

$$\phi(t) \to \phi(t) - \lim_{t\to+\infty}\phi(t).$$

Assume that for large t, $\phi(t)$ converges towards some non-zero constant ϕ_0. Then we can take the limit as

$$\lim_{t\to\infty}\phi(t) = \frac{1}{t}\int_0^t \phi(t) = \phi_0\frac{t}{t} = \phi_0,$$

and we get

$$\lim_{t\to\infty}\mathsf{Tr}\rho^0\big[H^1(0),B(t)\big] = \lim_{t\to\infty}\frac{1}{t}\int_0^t \mathsf{Tr}\rho^0\big[H^1(0),B(t')\big]\,dt' = \mathsf{Tr}\rho^0\big[H^0,B^0\big]$$

The zero-frequency component of the argument $\rho^0\big[H^1(0),B^0(t)\big]$ is simply its value before the perturbation. Our final result for the response function is therefore given by

$$\phi(t-t') = i\,\mathsf{Tr}\,\rho^0\big[H^1(t'),B(t-t')\big] - i\mathsf{Tr}\,\rho^0\big[H^0,B^0\big]. \tag{2.54}$$

Complex admittance, relaxation function and time-derivative

After the derivation of the explicit form of $\phi(t-t')$, Kubo proceeds in the third chapter of reference [1] by defining three quantities that are closely related to the response funtion. We shall do the same here, as they will prove to be helpful in the implementation of the Kubo-Green relation to compute the ionic polarisability.

First of all, consider the special case of the response function which we obtain when we apply a uniform perturbation $H^1(t) = H^1$ from $t = -\infty$ to $t = 0$. After the perturbation is switched off, the value of $B^1(t)$ will relax according to

$$B^1(t) = \int_{-\infty}^0 \phi(t-t')dt'.$$

We shift the integration variable according to $t' \to t - t'$, and we get

$$B^1(t) = -\int_\infty^t \phi(t')dt' = \int_t^\infty \phi(t')dt' \qquad \text{for} \qquad t > 0.$$

We call the quantity

$$\Phi(t) = \lim_{\eta\to 0^+}\int_t^\infty \phi(t')e^{-\eta t'}\,dt' \tag{2.55}$$

the relaxation function associated to $\phi(t)$, as it describes the relaxation of $B^1(t)$ after the perturbation is lifted. As we will see in a moment, $\Phi(t)$ can be thought of as the primitive function for $\phi(t)$.

Secondly, note that the time-derivative of $\phi(t)$ is given by

$$\dot\phi(t-t') = i\mathsf{Tr}\;\rho^0\big[H^1(t'),\dot B(t-t')\big]. \tag{2.56}$$

Thirdly, we define the complex admittance $\chi(\omega)$ as the (damped) Fourier transform of $\phi(t)$. Introducing a damping factor $e^{-\eta t}$, where $\eta \ll 1$, ensures convergence of the integral. The admittance $\chi(\omega)$ can be calulated by

$$\chi(\omega) = \lim_{\eta\to 0}\int_0^\infty \phi(t)e^{-i\omega t-\eta t}dt \tag{2.57}$$

Lastly, note that it is equally possible to define admittance functions that are associated to the responses $\Phi(t)$ and $\dot\phi(t)$, respectively:

$$X(\omega) = \lim \eta \to 0\int_0^\infty \Phi(t)e^{-i\omega t-\eta t}dt, \tag{2.58}$$

and

$$\dot{\chi}(\omega) = \lim \eta \to 0 \int_0^\infty \dot{\phi}(t) e^{-i\omega t - \eta t} dt, \tag{2.59}$$

where the dot in $\dot{\chi}$ is purely symbolic and does not indicate an actual time-derivative of the frequency-dependent admittance.

Remember that in frequency space, taking a derivative with respect to time amounts to a multiplication by $i\omega$, while an integral over time is the same as a division by $i\omega$. We can use this fact to relate the different admittance functions to one another:

$$\begin{aligned}\chi(\omega) &= \lim_{\eta\to 0} \int_0^\infty \phi(t) e^{-i\omega t - \eta t} dt \\ &= \lim_{\eta\to 0} \frac{1}{i\omega + \eta} \Big[\phi(0) + \int_0^\infty \dot{\phi}(t) e^{-i\omega t - \eta t} dt\Big] = \lim_{\eta\to 0} \frac{1}{i\omega + \eta} \Big[\dot{\phi}(0) + \dot{\chi}(\omega)\Big]\end{aligned} \tag{2.60}$$

and

$$\chi(\omega) = \lim_{\eta\to 0} \int_0^\infty \phi(t) e^{-i\omega t - \eta t} dt = \Phi(0) - i\omega \int_0^\infty \Phi(t) e^{-i\omega t} dt = \Phi(0) - i\omega X(\omega). \tag{2.61}$$

Response functions in a canonical ensemble

In this section, we will look at the results of the FD theorem in a canonical ensemble at temperature $T > 0K$. We will derive exact expressions for the response functions and the related quantities defined above and investigate the classical limit.

We use the density operator in the canonical ensemble,

$$\rho_\beta = \frac{e^{-\beta H^0}}{\mathsf{Tr}\ e^{-\beta H^0}}.$$

When computing the response function (cf. 2.52),

$$\phi(t - t') = -i\, \mathsf{Tr}\Big[\big[\rho_\beta, H^1(t')\big] B_I(t - t')\Big],$$

we encounter terms of the form $\big[e^{-\beta H^0}, H^1(t)\big]$. Applying Kubo's transformation (2.46), we obtain

$$\big[e^{-\beta H^0}, H^1(t)\big] = i\, e^{-\beta H^0} \int_0^\beta \dot{H}^1(t - i\tau)\, d\tau, \tag{2.62}$$

or indeed

$$\big[\rho_\beta, H^1(t)\big] = i\rho_\beta \int_0^\beta \dot{H}^1(t - i\tau)\, d\tau.$$

It follows that the response function of a system in the canonical ensemble is given by

$$\begin{aligned}\phi(t - t') &= i\mathsf{Tr}\ \Big[\big[\rho_\beta, H^1(t')\big] B(t - t')\Big] \\ &= -\int_0^\beta \mathsf{Tr}\ \Big[\rho_\beta \dot{H}^1(t' - i\tau) B(t - t')\Big] d\tau \\ &= \int_0^\beta \mathsf{Tr}\ \Big[\rho_\beta H^1(t' - i\tau) \dot{B}(t - t')\Big] d\tau.\end{aligned} \tag{2.63}$$

In the classical limit, the notion of imaginary time $i\tau$ vanishees, and also the inverse temperature $\beta = (k_B T)^{-1}$ becomes very small for $T \gg OK$. Therefore, we neglect the dependence on $i\tau$,

and to first order the integral gives a factor of β. Using again the definition of the phase space average in quantum theory, we obtain

$$\phi(t-t') = \beta\langle H^1(t')\dot{B}(t-t')\rangle = -\beta\langle \dot{H}^1(t')B(t-t')\rangle - \beta\langle H^0B^0\rangle. \tag{2.64}$$

Equation (2.64) will be the starting point for our calculation of the ionic polarisability.

To complete this section, we will also give the explicit forms of the relaxation function and the time-derivative of the response function.

With (2.55), we get

$$\Phi(t) = i\int_t^\infty \mathsf{Tr}\rho^0\big[B(t'), H^1(0)\big]dt' = i\int_t^\infty dt' \int_0^\beta d\tau\, \mathsf{Tr}\rho^0 H^1(-i\tau)B(t').$$

which in the classical limit becomes

$$\Phi(t) = \beta\langle H^1(0)B(t)\rangle - \beta\langle H^0B^0\rangle. \tag{2.65}$$

Finally, for the time-derivative of $\phi(t)$ in the canonical ensemble, we get

$$\dot{\phi}(t-t') = i\,\mathsf{Tr}\big[\rho^0, H^1(t)\big]\dot{B}(t-t') = i\,\mathsf{Tr}\rho^0\big[H^1(t'), \dot{B}(t-t')\big]$$

$$= (-i)\,\mathsf{Tr}\rho^0\big[\dot{H}^1(t'), B(t-t')\big] = -\int_0^\beta \mathsf{Tr}\rho^0\dot{H}^1(t'-i\tau)\dot{B}(t-t')\,d\tau,$$

and its classical limit simply becomes

$$\dot{\phi}(t-t') = -\beta\langle \dot{H}^1(0)\dot{B}(t-t')\rangle. \tag{2.66}$$

2.2.2 Derivation following Zwanzig: Electrical conductivity

After this rather abstract derivation, let us now take a different, more practical look at the FD Theorem. The following derivation was presented by Robert Zwanzig in his review of non-equilibrium statistical mechanics, published in the 1960s (see ref. [2]). Ideally, it will lead us to a more intuitive understanding of the theorem.

In this paper, Zwanzig makes a comparison of computing the electrical conductivity with an actual measurement of the conductivity of a material in an experiment. This works along the following lines:

We perform a measurement of an electric current along a conducting wire following the application of an external electric field. A series of measurements yields the following relation between the average electric current $\langle\mathbf{J}\rangle$ and the applied field:

$$\langle\mathbf{J}\rangle = \sigma\mathbf{E} + O(\mathbf{E}^2). \tag{2.67}$$

In the language of the FD theorem, the electric field $\mathbf{E}$ corresponds to a (small) perturbation $H^1(t)$ in the Hamiltonian , and $\mathbf{J}$ is represented by the observble $B(t)$ whose change we want to describe.

We rewrite (2.67) in the form

$$\langle\mathbf{J}\rangle = \int_0^t \phi(t-t')\mathbf{E}(t')dt' + O(\mathbf{E}^2),$$

with the response function $\phi(t)$. Transformation to Fourier space yields

$$\langle \mathbf{J}_\omega \rangle = \int_0^\infty e^{-i\omega t} \int_0^t \phi(t-t')\mathbf{E}(t')dt'dt.$$

We recognise that the conductivity $\sigma(\omega)$ is simply the complex admittance $\chi(\omega)$ associated with the response function $\phi(t)$, i.e. that

$$\sigma(\omega) = \int_0^\infty dt\, e^{-i\omega t}\phi(t),$$

and we have

$$\langle \mathbf{J}_\omega \rangle = \sigma(\omega)\mathbf{E}_\omega.$$

Now assume that we want to measure the electrical current through our piece of wire. We can describe such an experiment in three stages: the initial preparation of the system (described by the unperturbed Hamiltonian H^0), the switching-on of the field (i.e. the perturbation $H^1(t)$), and the measurement of the current.

Preparation of the system

As usual, we start from the unperturbed Hamiltonian H_0, whose eigenstates and eigenenergies are assumed to be known via

$$H^0|\Psi_n^0\rangle = E_n^0|\Psi_n^0\rangle.$$

The equilibrium Hamiltonian H^0 gives rise to the natural motion of the states $|\Psi_n^0\rangle$ in the usual way

$$|\Psi_n^0(t)\rangle = e^{-iH^0t}|\Psi_n^0\rangle, \tag{2.68}$$

causing the state $|\Psi_n^0(t)\rangle_S$ to explicitly depend on time. Note that in this sections, all states and operators are to be taken in the Schrödinger picture. We repeat the measurement many times at non-zero temperature $T > 0$. As we have seen in section (2.1.4), the actual state of the system can then be described by a mixed state

$$|\Psi\rangle = \sum_n e^{-\beta E_n^0}|\Psi_n^0(t)\rangle\langle\Psi_n^0(t)|$$

with the corresponding density matrix

$$\rho = \frac{e^{-\beta H^0}}{\mathrm{Tr}e^{-\beta H^0}}.$$

Switching on the field

Next, we perturb the system by applying some time-dependent external electric field $\mathbf{E}(t)$. The Hamiltonian of the perturbation can be written as

$$H^1(t) = -\mathbf{P}\cdot\mathbf{E}(t) = -\sum_{\alpha=1}^{3} P_\alpha E_\alpha(t),$$

where α is the index for the directions (x, y, z), and $\mathbf{P}$ is the total dipole moment of the system. We look for solutions of the perturbed time-dependent Schrödinger equation

$$i\frac{\partial|\Psi_n(t)\rangle}{\partial t} = \left[H^0 + H^1(t)\right]|\Psi_n(t)\rangle \tag{2.69}$$

with the initial condition

$$|\Psi_n(t=0)\rangle_I = |\Psi_n^0(t=0)\rangle_S = |\Psi_n^0\rangle.$$

We already solved this in equation (2.19):

$$|\Psi_n^0(t)\rangle = e^{-iH^0 t}|\Psi_n^0\rangle - i\int_0^t e^{-iH^0(t-t')}H^1(t')e^{-iH^0 t'}|\Psi_n^0\rangle dt'. \tag{2.19}$$

Using the closure relation

$$\mathbb{1} = \sum_m |\Psi_m^0\rangle\langle\Psi_m^0|,$$

we get to

$$|\Psi_n(t)\rangle = e^{-iE_n^0 t}|\Psi_n^0\rangle - i\sum_{m\neq n}\int_0^t e^{-iE_m^0(t-t')}H_{mn}^1 e^{-iE_n^0 t'}|\Psi_m^0\rangle dt', \tag{2.70}$$

which is the same as the equation on page 73 in [1].

Measurement of the Current With the knowledge of what the wavefunction looks like after the electric field has been switched on, we can compute the resulting current by averaging over the current operator in the basis of the new time-dependent mixed state $|\Psi(t)\rangle$ (cf. 2.48).

Remember that if $\mathbf{P}$ is the total dipole of a system, then $\mathbf{J} = \dot{\mathbf{P}}$ is the electric current resulting from the change of the dipole over time.

At first, let us write down the expectation value for J_α in a single pure (but time-dependent) state $|\Psi_n(t)\rangle$ of the ensemble. As always, we will neglect terms proportional to $\mathbf{E}^2$ and higher:

$$\langle J_\alpha(t)\rangle = \langle\Psi_n(t)|J_\alpha|\Psi_n(t)\rangle = \langle\Psi_n^0|J_\alpha|\Psi_n^0\rangle - i\sum_{m\neq n}\int_0^t (J_\alpha)_{nm}e^{-i(E_m^0-E_n^0)(t-t')}H_{mn}^1(t')dt'$$

$$+i\sum_{m\neq n}\int_0^t (J_\alpha)_{mn}e^{i(E_m^0-E_n^0)(t-t')}H_{nm}^1(t')dt'. \tag{2.71}$$

To describe the full canonical ensemble, we now have to average over all $|\Psi_n(t)\rangle$, weighted by the canonical density of states. That is, we turn (2.71) into the weighted sum

$$\langle J_\alpha(t)\rangle = \sum_n \rho_n^0\langle\Psi_n(t)|J_\alpha|\Psi_n(t)\rangle,$$

where we use the shorthand

$$\rho_n^0 = \frac{e^{-\beta E_n^0}}{\sum_m e^{-\beta E_m^0}}$$

for the statistical weight of the state with energy E_n^0. We continue,

$$\begin{aligned}\langle J_\alpha(t)\rangle &= \sum_n \rho_n^0\langle\Psi_n^0|J_\alpha|\Psi_n^0\rangle \\ &- i\sum_n \rho_n^0\sum_{m\neq n}\int_0^t \Big[e^{-i(E_m^0-E_n^0)(t-t')}(J_\alpha)_{nm}(P_\beta)_{mn} - e^{i(E_m^0-E_n^0)(t-t')}(J_\alpha)_{nm}(P_\beta)_{mn}\Big]E_\beta(t')dt'.\end{aligned} \tag{2.72}$$

In (2.72), we used that the perturbation is just $H^1(t) = \mathbf{P}\cdot\mathbf{E}(t)$, and that E_α, the electric field component in direction j, is a scalar factor. In the end, we want to write the result in the form

$$\langle J_\alpha(t)\rangle = \langle J_\alpha\rangle_{eq} + \int_0^t dt'\phi_{\alpha\beta}(t-t')E_\beta(t') \tag{2.73}$$

with the average current at equilibrium $\langle J_\alpha \rangle_{eq}$, and the after-effect function $\phi_{\alpha\beta}(t)$. By comparison of equations (2.72) and (2.73), we see that the equilibrium current $\langle J_\alpha \rangle_{eq}$ is equal to the first term in (2.72),

$$\langle J_\alpha \rangle_{eq} = \sum_n \rho_n^0 (J_\alpha)_{nn} = 0.$$

For this particular system, we can assume that the equilibrium current is zero. Furthermore, we can read off the definition of the response function,

$$\phi_{\alpha\beta}(t) = \sum_{\substack{n,m \\ m \neq n}} (-i)\rho_n^0 \Big[e^{-i(E_m^0 - E_n^0)t} (J_\alpha)_{nm} (P_\beta)_{mn} - e^{i(E_m^0 - E_n^0)t} (J_\alpha)_{nm} (P_\beta)_{mn} \Big]. \tag{2.74}$$

The matrix elements of the current, $(J_\alpha)_{mn}$, are computed with respect to the eigenvectors of H^0. This allows us to make the transformation

$$\begin{aligned} (J_\alpha)_{mn} &= \langle \Psi_m^0 | J_\alpha | \Psi_n^0 \rangle = \langle \Psi_m^0 | \dot{P}_\alpha | \Psi_n^0 \rangle = i \langle \Psi_m^0 | \big[H^0, P_\alpha \big] | \Psi_n^0 \rangle \\ &= i E_m^0 \langle \Psi_m^0 | P_\alpha | \Psi_n^0 \rangle - i E_n^0 \langle \Psi_m^0 | P_\alpha | \Psi_n^0 \rangle = i (E_m^0 - E_n^0) \langle \Psi_m^0 | P_\alpha | \Psi_n^0 \rangle. \end{aligned} \tag{2.75}$$

A similar consideration leads us to

$$\begin{aligned} e^{i(E_m^0 - E_n^0)t} (J_\alpha)_{mn} &= \langle \Psi_m^0 | e^{i E_m^0 t} \, J_\alpha \, e^{-i E_n^0 t} | \Psi_n^0 \rangle \\ &= \langle \Psi_m^0 | e^{i H^0 t} \, J_\alpha \, e^{-i H^0 t} | \Psi_n^0 \rangle = \big[J_\alpha(t) \big]_{mn}, \end{aligned} \tag{2.76}$$

where $J_\alpha(t)$ is the current operator in the interaction picture. With (2.75) and (2.76), we can simplify the response function to

$$\phi_{\alpha\beta}(t) = \sum_{\substack{n,m \\ m \neq n}} e^{-\beta E_n^0} (J_\alpha)_{mn} \big[J_\beta(t) \big]_{mn} \frac{e^{-\beta(E_n^0 - E_m^0)} - 1}{E_m^0 - E_n^0}. \tag{2.77}$$

We can re-write (2.77) using the integral

$$\phi_{\alpha\beta}(t) = i \sum_m \rho_m \int_0^\beta d\tau \, \big(J_\alpha(t') \big)_{nm} \big(J_\beta(-i\tau) \big)_{mn}. \tag{2.78}$$

In (2.78), $\phi(t)$ is identical to the result obtained in (2.63) but with the perturbation $H^1(t) = \mathbf{P} \cdot \mathbf{E}$, and the observable $B(t)$ is in this particular case the current $J(t)$. Following (2.64), we know the classical limit for the conductivity tensor, namely

$$\phi_{\alpha\beta}(t) = \beta \langle J_\alpha J_\beta(t) \rangle = \beta \langle \dot{P}_\alpha \dot{P}_\beta(t) \rangle. \tag{2.79}$$

Observe, that in (2.79), there is no constant offset to subtract, as we can reasonably assume that there is no current without an external electric field. With this, we have found the expression for the electric conductivity of a system of dipoles in terms of the equilibrium fluctuations of the total dipole moment

$$\sigma_{\alpha\beta}(\omega) = \beta \int_0^\infty \langle J_\alpha J_\beta(t) \rangle e^{-i\omega t} dt. \tag{2.80}$$

2.3 Linear response methods in solids

After the proof of the fluctuation-dissipation theorem, we now have to take a step back to discuss general linear response methods in solids. In the next chapter, we will derive the ionic polarisability in a crystal both from a Kubo-Green relation and using an already well-known method starting from the phonon spectrum. The main drawback of the phonon response function is that in an ordinary density-functional theory simulation, it can only give results for the ground-state of a system, that is at a temperatur of 0K, while Kubo-Green is in principle applicable at any temperature.

In the next chapter, we will show that the ground-state ionic polarisability obtained from the phonon spectrum can be obtained as a limiting case of the respective Kubo-Green relation, and in chapter 5, we will support this claim using simulations of the dielectric function of two perovskite systems in the groundstate and at higher temperatures.

Beforehand, however, we must discuss two basic ideas needed to understand the phonon response. In this section, we describe a crystal as a system of coupled oscillating dipoles. The application of an external electric field generally excites the dipole oscillators, and causes a time-dependent dipole field as a response to the initial perturbation.

Firstly, we will give a general - and very compact - overview of the theory of eigenmodes (phonon modes) in a periodic crystal. We will see how an excited ion in a periodic crystal can only move along a very specific direction, determined by its eigenmode, and only do so at particular frequency, its eigenfrequency.

Secondly, we will determine the dipole activity of the modes. This is equivalent to asking if the movement of an ion along an eigenmode leads to a displacement of electric charge within the unit cell, and if yes by how much. One would, for instance, expect strong dipole activity from a mode if it causes contraction and expansion of the bond length between two strongly polar atoms, for instance in an ionic bond. If, on the other hand, the motion of an ion along an eigenmode leaves the effective charge distribution in the cell unchanged, the mode is said to be not dipole-acitve. A measure for dipole activity (correct up to linear order) is provided by the 'Born effective charge' of an ion.

2.3.1 Phonons in solids

In this subsection, we will derive the dynamical matrix of a system in the harmonic approximation. As we will see further down, up to linear order, the eigenvectors of the dynamical matrix can be identified with the eigenmodes of the crystal. The corresponding eigenvalues give the eigenfrequencies of the oscillations. This subsection follows the derivation given in chapter 5 of ref. [4].

The position of an atom in a unit cell can be specified by

$$\mathbf{r}^{ni} = \mathbf{R}^n + \mathbf{r}^i,$$

where n is the unit cell index and i the index of the atom within the unit cell. Starting from the equilibrium configuration of the system, we can expand the total potential energy U for small displacements $\Delta\mathbf{r}^{in}$ into a series

$$U(\{\mathbf{r}^{ni}\}) = U_0 + \sum_{n,i,\alpha} \frac{\partial U}{\partial r_\alpha^{ni}} \Delta r_\alpha^{in} + \frac{1}{2} \sum_{\substack{n,m \\ i,j \\ \alpha,\beta}} \frac{\partial^2 U}{\partial r_\alpha^{ni}\, \partial r_\beta^{mj}} \Delta r_\alpha^{ni} \Delta r_\beta^{mj} + ...$$

Greek indices $\{\alpha, \beta, ...\}$ indicate the cartesian directions x, y and z. In equilibrium, the first derivatives $\partial U / \partial r_\alpha^{ni}$ must of course vanish. In the harmonic approximation, we neglect contribu-

tions from all higher derivatives of the energy, and we can express the potential energy as

$$U = U_0 + \frac{1}{2} \sum_{\substack{n,m \\ i,j \\ \alpha,\beta}} \frac{\partial^2 U}{\partial r_\alpha^{ni} \, \partial r_\beta^{mj}} \Delta r_\alpha^{ni} \Delta r_\beta^{mj}. \tag{2.81}$$

The second derivatives of the potential at the equilibrium position have dimensions of spring constants (elastic constants), and correspond to a generalisation of the spring constant of a harmonic oscillator to a system with more than one degree of freedom. We introduce the shorthand

$$C_{\alpha\beta}^{nimj} = \frac{1}{2} \frac{\partial^2 U}{\partial r_\alpha^{ni} \, \partial r_\beta^{mj}}$$

for the tensor of elastic constants of the crystal. If we know all the elastic constants of the system, and we were to displace atom j in cell m in direction β, we can give a straightforward expression for the resulting force on atom i of cell n in direction α, namely

$$F_\alpha^{ni} = -C_{\alpha\beta}^{nimj} \Delta r_\beta^{mj}. \tag{2.82}$$

For all real materials, the second derivatives appearing in (2.82) are generally non-zero, which means that the motion of a single particle always causes subsequent motion of all other particles. Therefore, any description of the dynamics of ions in a crystal must capture the collective motion of all N particles in the system.

To do so, write down an equation of motion for the N-particle system, which is just a generalised harmonic oscillator equation in terms of the displacements $\Delta\mathbf{r}$,

$$m_i \frac{\partial^2 \Delta r_\alpha^{ni}}{\partial t^2} + \sum_{m,j,\beta} C_{\alpha\beta}^{nimj} \Delta r_\beta^{mj} = 0, \tag{2.83}$$

where we introduced m_i, the mass of particle i.

In a crystal consisting of N atoms, equation (2.83) defines a system of $3N$ coupled differential equations. At first glance, this may seem like a big number, but the periodicity of the system will allow us to reduce the complexity of the problem. In a periodic system, we expect to be able to write the solution as a linear combination of plane waves of the form

$$\Delta r_\alpha^{ni} = \frac{1}{\sqrt{m_i}} a_\alpha^{ni}(\mathbf{q}) e^{i(\mathbf{q}\cdot\mathbf{R}^n - \omega t)},$$

where $\mathbf{q}$ is a vector in the reciprocal lattice. This family of plane waves is only defined at the grid points $\mathbf{R}$. Inserting this ansatz into (2.83) yields

$$-\omega^2 a_\alpha^{ni}(\mathbf{q}) + \sum_{mj,\beta} \frac{1}{\sqrt{m_i m_j}} C_{\alpha\beta}^{nimj} \, e^{i\mathbf{q}\cdot(\mathbf{R}^n - \mathbf{R}^m)} a_\beta^{mj}(\mathbf{q}) = 0 \tag{2.84}$$

Due to translation invariance, the exponent $e^{i\mathbf{q}\cdot(\mathbf{R}^n - \mathbf{R}^m)}$ only depends on the difference $\mathbf{R}^n - \mathbf{R}^m$. Summing over all m, we obtain

$$D_{\alpha\beta}^{ij}(\mathbf{q}) = \sum_m \frac{1}{\sqrt{m_i m_{i'}}} C_{\alpha\beta}^{nimj} e^{i\mathbf{q}\cdot\mathbf{R}^m}, \tag{2.85}$$

which is independent of the lattice index n. We call (2.85) the dynamical matrix of the system. We can use it to rewrite (2.84) as

$$-\omega^2 a_\alpha^{ni}(\mathbf{q}) + \sum_{m,j,\beta} D_{\alpha\beta}^{ij}(\mathbf{q}) a_\beta^{mj}(\mathbf{q}) = 0.$$

As in our expression for the dynamical matrix we have summed over all lattice vectors. The remaining expression is just a system of $3N_c$ equations, where N_c is the number of atoms in the unit cell, rather than of $3N$ equations, with N being the total number of atoms. The general solution of the equation of motion (2.83) is a linear combination of eigenvectors of the dynamical matrix (2.85).

We can conclude that, due to the interaction of all ions in the crystal via (2.82), only such movements of the ions are allowed which satisfy the equation of motion (2.83). Using the ansatz for plane waves in solids, we were able to set up the dynamical matrix, whose eigenvectors exactly satisfy the equation of motion. These eigenvectors of the dynamical matrix are called phonon modes.

2.3.2 Born effective charges

Following the derivation by Wu, Vanderbilt and Hamann in ref. [5], we generalise the core idea of the previous section, namely the series expansion of the potential energy, to arrive at an expression for the Born effective charges.

While in the previous subsection the perturbation is a field of displacements $\Delta\mathbf{r}^{ni}$, we can consider the total energy also to be a function of a (homogeneous) external electric field $\mathbf{E}$. As in the previous section, translation invariance in the crystal lattice will allow us to make general statements about the crystal lattice from considerations in the unit cell alone, so that we can omit the unit cell index n, and write the displacement as $\Delta\mathbf{r}^{i}$.

We will expand the potential energy U up to second order in powers of displacements and external electric field. After the series expansion, we can systematically define all response properties as derivatives of the energy U per unit volume with respect to the perturbations.

To ensure consistency of all derived quantities we have to introduce a small modification to the definition of the total energy (see [5]). In the presence of an external electric field, U becomes an electric enthalpy per (undeformed) volume Ω, and is thus given by

$$U(\Delta\mathbf{r}, \mathbf{E}) = \frac{U^0 - \mathbf{E}\cdot\mathbf{P}}{\Omega},$$

where U^0 is the initial potential energy in a vanishing field, and $\mathbf{P}$ is the total dipole moment in the unit cell.

We can expand the total energy in powers of $\Delta\mathbf{r}$ and $\mathbf{E}$,

$$\begin{aligned} U(\Delta\mathbf{r}, \mathbf{E}) = U^0 + \sum_i \Bigg[& \frac{\partial U}{\partial r^i_\alpha}\Delta r^i_\alpha + \frac{\partial U}{\partial E_\alpha}E_\alpha \\ & + \frac{1}{2}\frac{\partial^2 U}{\partial r^i_\alpha \partial r^j_\beta}\Delta r^i_\alpha \Delta r^j_\beta + \frac{1}{2}\frac{\partial^2 U}{\partial r^i_\alpha \partial E_\beta}\Delta r^i_\alpha E_\beta + \frac{1}{2}\frac{\partial^2 U}{\partial E_\alpha \partial E_\beta}E_\alpha E_\beta \Bigg] + \ldots \end{aligned} \tag{2.86}$$

In fact, we can associate known quantities to most first and second derivatives appearing in (2.86). These are

$$
\begin{aligned}
F_\alpha^i =& \Omega \frac{\partial U}{\partial r_\alpha^i}, && \text{the force on particle i in direction } \alpha \text{ after displacement } \Delta r_\alpha^i, \\
P_\alpha =& \Omega \frac{\partial U}{\partial E_\alpha}, && \text{the dipole moment in direction } \alpha, \\
C_{\alpha\beta}^{ij} =& \frac{\Omega}{2} \frac{\partial^2 U}{\partial r_\alpha^i \partial r_\beta^j}, && \text{the matrix of elastic constants, and} \\
\chi_{\alpha\beta} =& \Omega \frac{\partial^2 U}{\partial E_\alpha \partial E_\beta}, && \text{the ionic polarisability tensor.}
\end{aligned}
$$

In addition, we define the Born effective charge tensor $Z_{\alpha\beta}$ as

$$
Z_{\alpha\beta} = -\Omega \frac{\partial^2 U}{\partial r_\alpha^i \partial E_\beta} = -\frac{\partial P_\beta}{\partial r_\alpha^i}. \tag{2.87}
$$

According to equation (2.87), the Born effective charge is defined as the change of the dipole moment in direction α caused by a displacement of an atom in direction i. The full expansion of U up to second order corrections is therefore given by

$$
\begin{aligned}
U(\Delta \mathbf{r}, \mathbf{E}) = U^0 + \frac{1}{\Omega} \sum_{i,\alpha} \left[F_\alpha^i \Delta r_\alpha^i - P_\alpha E_\alpha \right] \\
+ \frac{1}{\Omega} \sum_{\substack{i,j \\ \alpha\beta}} \left[C_\alpha^{ij} \beta \Delta r_\alpha^i \Delta r_\beta^j + Z_{\alpha\beta} \Delta r_\alpha^i E_\beta + \frac{1}{2} \chi_{\alpha\beta} E_\alpha E_\beta \right] + ...
\end{aligned}
$$

Chapter 3

Ionic polarisability in solids

The purpose of this thesis is to present with the Kubo-Green relations for many-particle systems a more general method to determine the first-order dielectric response at non-zero temperature. In this chapter, we introduce the specific equations for the ionic polarisability as derived from Kubo-Green, we demonstrate how the limiting case of a delta-like perturbation leads to a great reduction in the computational demands when using Kubo-Green at or close to zero temperature, and we show that the ground-state phonon response can be obtained from the central formula of the fluctuation-dissipation theorem.

3.1 Kubo-Green relation for the ionic polarisability

3.1.1 Ionic polarisability from Kubo-Green

If we introduce a piece of matter into an external electric field **E**, the resulting field **D** inside the material follows the equation (in the CGS system)

$$\mathbf{D} = \mathbf{E} + 4\pi\mathbf{P}.$$

Here, **P** is the total induced dipole which appears as a response to the external field **E**. Another way of denoting this relation is by means of the dielectric function $\epsilon(\omega)$ through

$$\mathbf{D} = \epsilon(\omega)\mathbf{E}.$$

In general, the dielectric function is a tensorial quantity, and we will write it as

$$\epsilon_{\alpha\beta}(\omega) = \delta_{\alpha\beta} + \frac{4\pi e^2}{\Omega}\chi_{\alpha\beta}(\omega), \tag{3.1}$$

where e is the unit charge, Ω is the unit cell volume, and $\chi_{\alpha\beta}(\omega)$ is the frequency-dependent polarisability, defined in the previous section via

$$\chi_{\alpha\beta} = \Omega\frac{\partial^2 U}{\partial E_\alpha \partial E_\beta} = \frac{\partial P_\alpha}{\partial E_\beta}.$$

In particular, this implies the relation

$$\langle\mathbf{P}\rangle = \chi(\omega)\mathbf{E} + O(\mathbf{E}^2),$$

which is very similar to the definition of the electric conductivity

$$\langle\mathbf{J}\rangle = \sigma(\omega)\mathbf{E} \tag{2.67}$$

Note the connection between $\sigma_{\alpha\beta}$ and $\chi_{\alpha\beta}$ via

$$\frac{\partial\mathbf{P}(t)}{\partial t} = \mathbf{J}(t). \tag{3.2}$$

In analogy to the derivation in the Zwanzig paper, we compute $\langle\Psi(t)|P_\alpha|\Psi(t)\rangle$, i.e. we 'measure' the change of the dipole after the perturbation by the external electric field. We get

$$\begin{aligned}\langle P_\alpha(t)\rangle &= \langle\Psi_n^0(t)|P_\alpha|\Psi_n^0(t)\rangle \\ &= \langle\Psi_n^0|P_\alpha|\Psi_n^0\rangle - i\sum_{m\neq n}\int_0^t (P_\alpha)_{nm}e^{-i(E_m^0-E_n^0)(t-t')}H_{mn}^1(t')dt' \\ &\qquad + i\sum_{m\neq n}\int_0^t (P_\alpha)_{mn}e^{-i(E_n^0-E_m^0)(t-t')}H_{nm}^1(t')dt'.\end{aligned}$$

This time, the response function $\phi(t)$ must be

$$\phi_{\alpha\beta}(t) = -i\sum_{\substack{n,m\\ m\neq n}} e^{-\beta E_n^0}\Big[e^{-i(E_m^0-E_n^0)t}(P_\alpha)_{nm}(P_\beta)_{mn} - e^{i(E_n^0-E_m^0)t}(P_\alpha)_{nm}(P_\beta)_{mn}\Big],$$

and after the same maniuplations as above, we obtain for the classical limit the expression

$$\phi_{\alpha\beta}(t) = \beta\langle J_\alpha(0)P_\beta(t)\rangle = \beta\langle\dot{P}_\alpha(0)P_\beta(t)\rangle. \tag{3.3}$$

The admittance function is therefore given by

$$\chi_{\alpha\beta}(\omega) = \beta\int_0^\infty \langle\dot{P}_\alpha(0)P_\beta(t)\rangle e^{-i\omega t}dt, \tag{3.4}$$

or indeed by

$$\chi_{\alpha\beta}(\omega) = \beta\int_0^\infty \langle J_\alpha(0)P_\beta(t)\rangle e^{-i\omega t}. \tag{3.5}$$

Comparing (3.5) with the Kubo equation

$$\phi(t-t') = \beta\langle H^1(t')\dot{B}(t-t')\rangle - \beta\langle H^0B^0\rangle = -\beta\langle\dot{H}^1(t')B(t-t')\rangle - \beta\langle H^0B^0\rangle, \tag{2.64}$$

we see that the relevant observable $B(t)$ to compute the polarisability is the total dipole moment $\mathbf{P}(t)$ of the unit cell. The Hamiltonian for the perturbation by an external electric field is, as before,

$$H^1(t) = \mathbf{P}\cdot\mathbf{E}(t).$$

3.1.2 Equivalent dielectric functions

Comparing the response functions related to the conductivity (2.79) and the polarisability (3.3),

$$\sigma_{\alpha\beta}: \qquad \phi_{\alpha\beta}(t) = \beta\langle\dot{P}_\alpha(0)\dot{P}_\beta(t)\rangle,$$

$$\chi_{\alpha\beta}: \qquad \phi_{\alpha\beta}(t) = \beta\langle\dot{P}_\alpha(0)P_\beta(t)\rangle$$

it is clearly visible that one is the time derivative of the other. We could already expect this from equation (3.2). In other words, we can associate the conductivity $\sigma_{\alpha\beta}(\omega)$ to the admittance of the time-derivative of the response function defined in equation (2.59).

In linear response theory, in linear response theory, one can distinguish between *density-density* correlation, *density-current* correlation, or *current-current* correlation (see ref. [6]). In the framework of Kubo-Green, this nomenclature is reflective of the actual correlation function used to determine the response function.

For instance, if the perturbation is of the form $H^1(t) = \mathbf{P} \cdot \mathbf{E}(t)$, and we correlate the perturbation with the induced dipole $\mathbf{P}(t)$, we obtain the density-density correlation function of the system

$$\chi^{\rho\rho}_{\alpha\beta}(\omega) = \chi_{\alpha\beta}(\omega) = \beta \int_0^\infty \langle P_\alpha(0)\dot{P}_\beta(t)\rangle e^{-i\omega t} dt. \tag{3.6}$$

Bear in mind that the Kubo transformation introduces one extra time-derivative.

Equivalently, the case of the electric conductivity $\sigma_{\alpha\beta}$, we correlated the perturbation with the current $\mathbf{J}(t)$ induced in the system, giving rise to the density-current correlation function

$$\chi^{\rho\mathbf{j}}_{\alpha\beta}(\omega) = \sigma_{\alpha\beta}(\omega) = \beta \int_0^\infty \langle J_\alpha(0)\dot{P}_\beta(t)\rangle e^{-i\omega t} dt. \tag{3.7}$$

As established in section (2.2.1), these correlation functions are related to one another, as well as to the primitive correlation function

$$X_{\alpha\beta}(\omega) = \beta \int_0^\infty \langle P_\alpha(0)P_\beta(t)\rangle e^{-i\omega t} dt, \tag{3.8}$$

through

$$\chi^{\rho\mathbf{j}}(\omega) = i\omega\, \chi^{\rho\rho}(\omega) = -\omega^2 X(\omega) \tag{3.9}$$

and

$$X(\omega) = \frac{1}{i\omega}\, \chi^{\rho\rho}(\omega) = -\frac{1}{\omega^2}\, \chi^{\rho\mathbf{j}}(\omega). \tag{3.10}$$

3.2 Delta pulse method

The results of the fluctuation-dissipation theorem are valid up to linear order irrespective of the exact shape or duration of the perturbation. One can use this fact and try to find a function for the external perturbation which simplifies the computation of a response function.

Possibly the greatest simplification can be achieved by using a perturbing potential that is delta-like in time. Take the example of the density-density correlation function $\chi^{\rho\rho}(\omega)$ which connects the polarisability $\mathbf{P}$ to an external electric field $\mathbf{E}(t)$. For the dipole moment $\mathbf{P}$ we have the relationship (cf. 2.73)

$$\langle \mathbf{P}(t) \rangle = \langle \mathbf{P} \rangle_{eq} + \int_0^t dt' \phi(t-t') \mathbf{E}(t'),$$

which we rewrite as

$$\langle \mathbf{P}(t) \rangle - \langle \mathbf{P} \rangle_{eq} = \int_0^t dt' \phi(t-t') \mathbf{E}(t').$$

We know that the Fourier transform of $\phi(t)$ is

$$\chi^{\rho\rho}(\omega) = \int_0^\infty dt\, \phi(t) e^{-i\omega t}.$$

In order to determine the electric susceptibility of the material, we will apply a homogenous electric field for an infinitesimally short amout of time, i.e. $\mathbf{E} = \mathbf{E}_0\, \delta(t)$, and keep track of the change of the polarisation of the material $\mathbf{P}(t)$. We have

$$\langle \mathbf{P}(t) \rangle - \langle \mathbf{P} \rangle_{eq} = \int_0^t dt'\, \phi(t-t') \mathbf{E}_0\, \delta(t') = \phi(t) \mathbf{E}_0. \tag{3.11}$$

In order to get rid of the dipole moment in equilibrium, we apply another delta pulse of the same magnitude in the opposite direction. A non-zero equilibrium dipole will cause the response function obtained after the second pulse to differ from the one in equation (3.11). We indicate this by writing $\tilde{\phi}(t)$:

$$\langle \tilde{\mathbf{P}}(t) \rangle + \langle \mathbf{P} \rangle_{eq} = -\tilde{\phi}(t) \mathbf{E}_0. \tag{3.12}$$

We add equations (3.11) and (3.12), divide by the field strength

$$\frac{\langle \mathbf{P}(t) \rangle + \langle \tilde{\mathbf{P}}(t) \rangle}{\mathbf{E}_0} = \phi(t) - \tilde{\phi}(t)$$

and define the total response function as

$$\phi^{tot}(t) = \frac{1}{2}\big(\phi(t) - \tilde{\phi}(t)\big),$$

so that in the limit of $\langle \mathbf{P}(t) \rangle_{eq} = 0$ we simply get $\phi^{tot}(t) = \phi(t)$. Having obtained a simple expression for the response function,

$$[\phi^{tot}(t)]_{\alpha\beta} = \frac{P_\alpha(t) + \tilde{P}_\alpha(t)}{2E_{0,\beta}},$$

all that is left to do is a transformation to frequency space:

$$[\chi^{\rho\rho}(\omega)]_{\alpha\beta} = \int_0^\infty dt\, [\phi^{tot}(t)]_{\alpha\beta} e^{-i\omega t} = \frac{1}{2E_{0,\beta}} \int_0^\infty dt\, \big(P_\alpha(t) + \tilde{P}_\alpha(t)\big) e^{-i\omega t} \tag{3.13}$$

3.3 Phonon response

Lastly, we want to recover the formula for the phonon response as implemented in VASP (see ref. 3.26) from a limiting case of Kubo-Green.

First, we derive the relation for a single harmonic oscillator. To compute the dielectric response $\chi(\omega)$ via the Kubo relation

$$\chi(\omega) = \int_0^\infty \langle p(0)\dot{p}(t)\rangle e^{-i\omega t} dt, \tag{3.6}$$

we need an approximation for the dipole moment $p(t)$. We assume

$$p(t) = Zr(t), \qquad \text{where} \qquad r(t) = a\cos(\omega' t + \phi),$$

the factor ω' is the eigenfrequency of the oscillator, and Z is its Born effective charge in units of the elementary charge e. To determine the maximum elongation a, we remind ourselves that in a canonical ensemble at temperature $T > 0\ K$, the equipartition theorem states that the average potential energy of a single independent harmonic oscillator is just

$$\langle U\rangle = \frac{1}{2}k_B T = \frac{1}{2\beta}. \tag{3.14}$$

At the same time, we also know that the relation

$$\langle U\rangle = \frac{1}{2}m\omega'^2\langle r^2(t)\rangle = \frac{1}{2}m\omega'^2\langle a^2\cos^2(\omega' t + \phi)\rangle = \frac{1}{4}m\omega'^2 a^2 \tag{3.15}$$

holds for the potential energy of a harmonic oscillator, where m is the oscillating mass and ω' is again the eigenfrequency of the oscillator. We conclude that the position coordinate of the harmonic oscillator follows the trajectory

$$r(t) = \sqrt{\frac{2}{\beta m\omega'^2}}\cos(\omega' t + \phi). \tag{3.16}$$

Note that the factor

$$a = \sqrt{\frac{2}{\beta m\omega'^2}} \tag{3.17}$$

does indeed have the dimension of length. The dipole $p(t)$ is given by

$$p(t) = Z\sqrt{\frac{2}{\beta m\omega'^2}}\cos(\omega' t + \phi). \tag{3.18}$$

In this simple case, the Born effective charge tensor Z is simply the actual charge of the harmonic oscillator. The time-derivative of the dipole is given by

$$\dot{p}(t) = -Z\sqrt{\frac{2}{\beta m}}\sin(\omega t' + \phi) \tag{3.19}$$

To evaluate the time-average $\langle p(0)\dot{p}(t)\rangle$, we integrate over one period of the oscillation and divide by the factor 2π. The arbitrary phase factor ϕ is eliminated in the course of the integration. We get

$$\begin{aligned}\langle p(0)\dot{p}(t)\rangle &= \frac{1}{2\pi}\frac{-2Z^2}{\beta m\omega'}\int_0^{2\pi}\cos(\omega' t')\sin(\omega'(t+t'))dt' \\ &= \frac{-Z^2}{\beta m\omega'}\sin(\omega' t) + \frac{1}{4\pi}\frac{Z^2 e^2}{\beta m\omega'^2}\Big[\cos(\omega'(t+4\pi)) - \cos(\omega' t)\Big]\end{aligned} \tag{3.20}$$

According to Kubo, we obtain the dielectric function $\chi(\omega)$ if we multiply (3.20) by β and compute its damped Fourier transformation. Later on, we will only only be interested in the imaginary part coming out of the Fourier transformation of the sine, so that we can write

$$\begin{aligned}\chi(\omega) &= \lim_{\eta\to 0}\int_0^\infty \beta\langle p(0)\dot{p}(t)\rangle e^{-i\omega t-\eta t}dt \\ &= \lim_{\eta\to 0}\int_0^\infty \beta\frac{-Z^2}{\beta m\omega'}\sin(\omega' t)e^{-i\omega t-\eta t}dt \\ &= \lim_{\eta\to 0}\frac{Z^2}{m\omega'}\int_0^\infty \frac{1}{2}\Big[e^{i\omega' t}-e^{-i\omega' t}\Big]e^{-i\omega t-\eta t}dt \\ &= \lim_{\eta\to 0}\frac{Z^2}{2m\omega'}\int_0^\infty \Big[e^{i(\omega'-\omega+i\eta)t}-e^{-i(\omega'+\omega-i\eta)t}\Big]dt. \end{aligned} \tag{3.21}$$

After the intergration, we obtain

$$\chi(\omega) = \lim_{\eta\to 0}\frac{Z^2}{2m\omega'}\left[\frac{1}{\omega'-\omega+i\eta}+\frac{1}{\omega+\omega'+i\eta}\right] \tag{3.22}$$

Equation (3.22) is our result for the dielectric function of a single harmonic oscillator with mass m and charge Z.

The next step is to generalise this result for the case of a cystalline system with n atoms and N phonon modes in a unit cell of volume Ω. To determine the dielectric admittance $\chi(\omega)$, we have to sum over all phonon modes $(a)^\nu$. Furthermore, we must keep track of the effective charge displaced by one single phonon mode $(a)^\nu$, which is achieved by replacing the particle charge Z by the expression

$$\sum_{i,\alpha} Z^i_{\beta\alpha}(a^i_\alpha)^\nu, \tag{3.23}$$

where $Z^i_{\beta\alpha}$ is again the Born effective charge in direction α caused by a displacement a^i_α of ion i in direction β. The mass of ion i is m_i. With these modifications, the expression for the polarisability of an n-particle system is

$$\chi_\alpha(\omega) = \sum_{i,\nu}\frac{|Z^i_{\alpha\beta}(a^i_\beta)^\nu|^2}{2m_i\,\omega'_\nu}\left[\frac{1}{\omega'_\nu-\omega+i\eta}+\frac{1}{\omega+\omega'_\nu+i\eta}\right]. \tag{3.24}$$

Equation (3.24) is essentially the same as the formula used in VASP to compute the phonon response function. A full discussion of this can be found in [7]. The actually implemented formula does not compute the polarisability $\chi(\omega)$ as defined in (3.1), but rather the dimensionless ratio between external field **E** and induced field **D**, that is

$$\hat{\chi}_{\alpha\beta} = \epsilon_{\alpha\beta} - \delta_{\alpha\beta},$$

where the ratio $\hat{\chi}$ is related to our polarisability χ via

$$\hat{\chi}_{\alpha\beta} = \frac{4\pi e^2}{\Omega}\chi_{\alpha\beta}. \tag{3.25}$$

In (3.25), the factor Ω is the volume of the unit cell, making $\hat{\chi}$ a dimensionless response function per unit volume. Together with (3.24), we finally obtain the phonon response function for an infinite crystal at zero temperature as

$$\hat{\chi}_\alpha(\omega) = \frac{4\pi e^2}{\Omega}\sum_\nu\frac{|Z^i_{\alpha\beta}(a^i_\beta)^\nu|^2}{2m_i\,\omega'_\nu}\left[\frac{1}{\omega'_\nu-\omega+i\eta}+\frac{1}{\omega+\omega'_\nu+i\eta}\right]. \tag{3.26}$$

Chapter 4

Implementation

In the previous chapter, we derived three independent methods for describing the linear response of a polarisable material to an external electrical field. Now, we will test these methods on a selection of crystalline systems with interesting electronic properties. More specifically, we run a series of computer simulations using a code package for Density-Functional Theory (DFT) simulations, namely the Vienna Ab-Initio Simulation Package, or VASP (see [8], [9] and [10]).

Using VASP, we will simulate the time-evolution of three example systems in a canonical ensemble, both in the groundstate and at non-zero temperature. The most basic function of VASP is the computation of the DFT groundstate energy of an infinite crystal. Starting from the groundstate energy, it can compute the inter-atomic forces within the unit cell, which in turn can be used for the time-integration in a simulation of the molecular dynamics (MD simulation). We will describe the time-evolution of our example systems in such an MD simulation.

At first, we give a brief introduction on the functionality of the simulation package. Next, we present the example systems and how the respective simulations have been initialised. Finally, we discuss the actual implementation of the Kubo-Green relation, the delta pulse method and the phonon response for the calculation of the ionic polarisability.

At the beginning of every simulation in VASP, we compute the DFT-groundstate energy of the considered system. For such a computation, one has to supply four input files, called INCAR, POSCAR, POTCAR and KPOINTS.

The INCAR file is used to control all free parameters of the calculation, such as the DFT iteration algorithm, the convergence threshold, the cutoff-energy, etc.

In POSCAR, one enters the lattice vectors of the crystal, as well as the coordinates and atom types of the ions in the unit cell.

The atom types in POSCAR must match the pseudopotentials in the POTCAR file. These pseudopotentialsprovide the input about the ions in terms of a projector-augmented wave potential (PAW).

Finally, one needs to specify the number of k-points in the reciprocal space on which the wavefunction should be computed. This is done in the KPOINTS file.

4.1 Initialisation of the test systems

4.1.1 A simple model: α-SiO_2

At first, we consider silicon dioxide in its α-phase (α-SiO_2), which is a very well-studied material and has the advantage of having a very stable structure from the ground state up to very high temperatures of around 840 K. As we will see later on, stability of the structure is an important property when applying the delta pulse to the system, as a very large pulse may move an unstable system to a new local potential minimum.

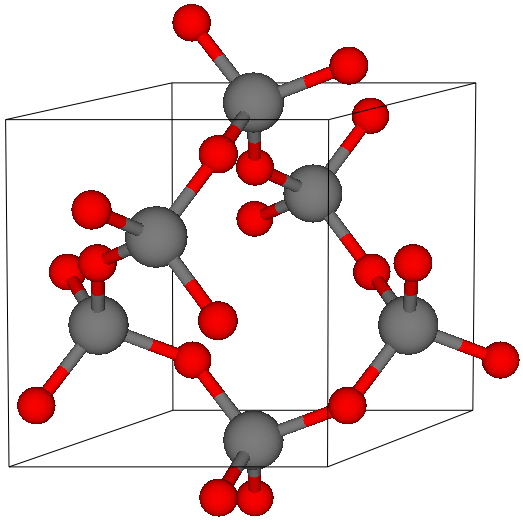

Figure 4.1: α-SiO_2 in a monoclinic unit cell.
Note that SiO_2 is symmetric under rotations of 60° in the xy-plane.

All images of crystals were produced using the free visualisation software VESTA, see ref. [11]. The initial structure of the right-handed $P3_121$ α-quartz structure was taken from [12]. We consider three SiO_2 units in a monoclinic supercell, with lattice parameters and atomic positions given in the table below.

lattice constants			angles		
a	b	c	α	β	γ
4.914	4.914	5.406	120°	60 °	90 °

atomic positions

atom type	Wyckoff symbol	fractional coordinates
Si	3a	(0.4648 0.0000 0.3333)
O	6c	(0.4104 0.2751 0.2206)

For silicon, we used the PBE PAW pseudopotential including both the $2s$ and $2p$ orbitals in the valence with an energy cutoff of 500 eV; for oxygen, we also used a PBE pseudopotential including the $2s$ and $4p$ orbitals. All calculations were performed with very strict convergence criteria, the convergence energy was set at 10^{-8} eV, and the force convergence threshold at 10^{-3} eV/Å. Given the size of the unit cell, a $2 \times 2 \times 2$ k-point grid was used.

The initial structure was relaxed using a conjugate-gradient method for ionic and volume relaxation. A useful test to assess the stability of the ground state can be a calculation of the phonons following the structural relaxation. At the stable potential energy minimum configuration, the dynamical matrix (2.85), i.e. the matrix of second-order derivatives of the energy with

respect to ionic displacements must be positive definite, indicating a point of positive curvature in the energy landscape.

As the eigenvalues of a positive definite matrix can only assume positive values, one should only expect real phonon eigenfrequencies. Imaginary phonon eigenfrequencies in the spectrum of the dynamical matrix hint at a structural instability in the configuration. Indeed, for our relaxed SiO_2 structure, we only found positive eigenfrequencies.

4.1.2 A simple perovskite system: $BaTiO_3$

Barium titanate ($BaTiO_3$ or BTO) has a perovskite structure and is an interesting material for its strong polarity and its flat potential energy surface around the potential minimum, which makes it very unstable.

At high temperatures (> 400K), BTO appears in its cubic phase (see ref. [13]), with six oxygen atoms forming an octahedron within the cubic cell. The centre of the octahedron is occupied by a titanium atom. The main instability of BTO stems from the fact that the central titanium atom is actually too small to occupy the whole space inside the octahedron. Furthermore, there exists a strong dipole between the Ti and O atoms, which, at temperatures below 400K, leads to a displacement of the titanium along one of the lattice vectors, thereby spontaneously breaking the cubic symmetry. The recovered phase has tetragonal symmetry. This effect is referred to as ferroelectric distorsion. At 278K, a second phase transition leads to another displacement of the titanium along a second lattice vector, yielding the orthorhombic phase of BTO. In other words, the central atom is now displaced along one face diagonal of the cube. Finally, at temperatures below 183K, BTO is rhombohedral, with the titanium atom displaced along the space diagonal of the cube.

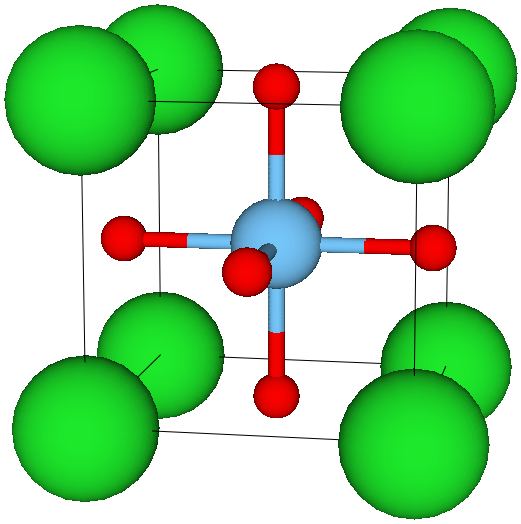

Figure 4.2: cubic $BaTiO_3$
The 6-fold cubic symmetry is intact, but we observe three imaginary modes.

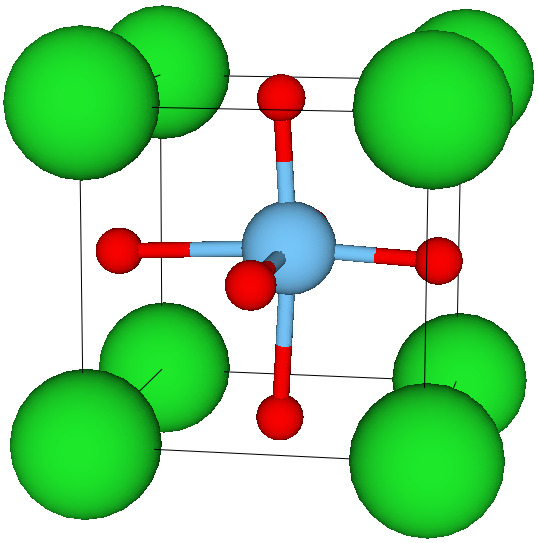

Figure 4.3: rhombohedral $BaTiO_3$.
Note the displacement of the central titanium atom along $[1, 1, 1]$.

The cubic structure of $BaTiO_3$, which will serve as a starting structure for all high-temperature MD simulations, was taken from ref. [14]. After initial relaxation, the lattice parameters for the cubic structure are given in the table below.

lattice constants			angles		
a	b	c	α	β	γ
4.028	4.028	4.028	90°	90 °	90 °

atomic positions

atom type	Wyckoff symbol	fractional coordinates
Ba	1a	(0.000 0.000 0.000)
Ti	1b	(0.500 0.500 0.500)
O	3c	(0.500 0.500 0.000)

Next to the cubic structure, we also need the true groundstate structure of BTO. Starting from the cubic configuration, the central Ti atom was displaced in the $[1, 1, 1]$-direction. Then, the cell shape, but not the ionic positions, was relaxed, followed by a relaxation of the volume and the ions, respectively. This relaxation procedure was iterated several times until convergence was reached. The final rhombohedral structure is indeed lower in energy than the cubic structure, with an energy difference of 97.25 meV in the simple unit cell. It has the following lattice parameters:

lattice constants			angles		
a	b	c	α	β	γ
4.071	4.071	4.071	89.68°	89.68 °	89.68 °

atomic positions

atom type	Wyckoff symbol	fractional coordinates
Ba	1a	(0.000 0.000 0.000)
Ti	1a	(0.484 0.484 0.484)
O	3b	(0.028 0.484 0.484)

For barium, a PBE pseudopotential including the $5s$, $5p$, and $6s$ orbitals was used; titanium was simulated using a PBE pseudopotential with $3s$, $3p$, $4s$, and $3d$ orbitals included, and for oxygen, we considered, as above, the $2s$ and $4p$ orbitals. The energy cutoff was set at 500 eV and the convergence threshold was 10^{-8} eV/Å. In the relaxation runs, the force convergence was set to be reached at 10^{-3} eV, and the accuracy of the force calculations was increased by setting PREC=Accurate. In the single unit cell, a $4 \times 4 \times 4$ k-point grid is used, while in the $2 \times 2 \times 2$ supercell, we use a $2 \times 2 \times 2$ k-point grid. This implies that we have the same k-point density in both cells.

While the fully relaxed rhomohedral structure exhibits no imaginary phonon modes and is therefore (locally) stable, the cubic structure suffers from 3 imaginary modes, i.e. there are three possible displacements of atoms that would lead to a lower total energy.

4.1.3 The unstable system: $SrTiO_3$

Strontium titanate ($SrTiO_3$ or STO) also belongs to the class of perovskites, and a priori has properties which are very similar to barium titanate. As before, we have three phase transitions, from cubic to tetragonal, from tetragonal to orthorhombic, and from orthorhombic to rhombohedral, which are related to the ferro-electric instabilities of the TiO_3 cage.

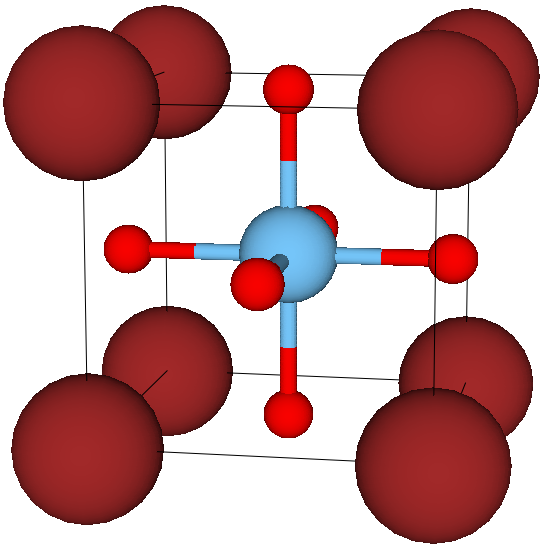

Figure 4.4: cubic $SrTiO_3$
The 6-fold cubic symmetry is intact, but we observe three imaginary phonon modes.

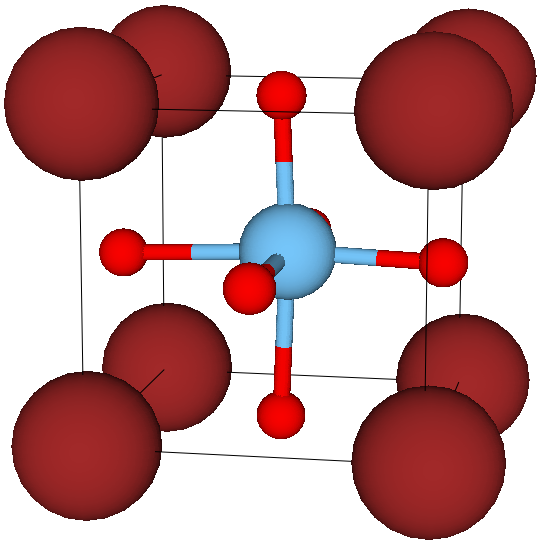

Figure 4.5: rhombohedral $SrTiO_3$
Note the displacement of the central titanium atom along $[1, 1, 1]$.

However, there is another complication: The strontium atoms in $SrTiO_3$ are equivalent to the barium atoms in $BaTiO_3$, but due to their lower atomic number, they are smaller and lighter than barium. This introduces another instability in the system, called anti-ferroelectric distorsion (see [14]). This distorsion amounts to a rotation of the O-octahedra in neighbouring unit cells in clockwise and anticlockwise direction around the O-Ti-O axis, respectively. As the rotation in any cell is always opposite the rotation in any cell next to it, this distorsion is only possible in $\sqrt{2} \times \sqrt{2} \times 1$ or even larger supercells.

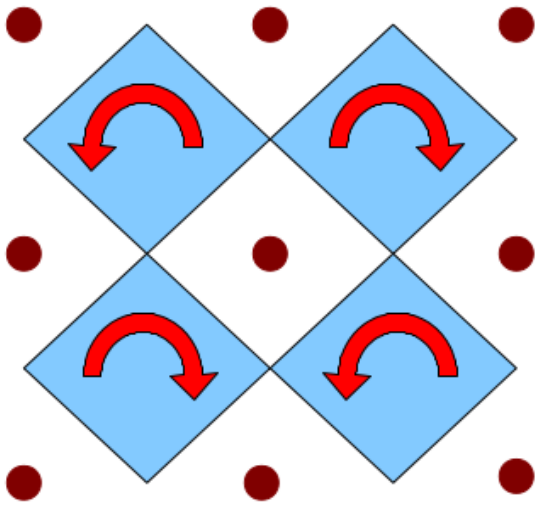

Figure 4.6: Anti-ferroelectric distorsion can only appear in a supercell where ions of neighbouring cells can move in opposite directions.

To initialise the structure of $SrTiO_3$, we start from the cubic structure given in [14]. After a first structural relaxation, the lattice parameters for the cubic structure of STO are given below.

lattice constants			angles		
a	b	c	α	β	γ
3.936	3.936	3.936	90°	90 °	90 °

atomic positions

atom type	Wyckoff symbol	fractional coordinates
Sr	1a	(0.000 0.000 0.000)
Ti	1b	(0.500 0.500 0.500)
O	3c	(0.500 0.500 0.000)

As for BTO, we then also create the rhombohedral groud-state structure by displacing the central Ti atom along the space diagonal. With an energy cutoff of 500 eV and an energy convergence threshold of 10^{-8} eV, we first relax the cell shape, then the volume, then the ionic positions. The force convergence threshould is set at 10^{-3} eV/Å, and the accuracy of the force calculation is increased. The resulting lattice parameters are then given by

lattice constants			angles		
a	b	c	α	β	γ
3.950	3.950	3.950	89.91 °	89.91 °	89.91 °

atomic positions

atom type	Wyckoff symbol	fractional coordinates
Sr	1a	(0.000 0.000 0.000)
Ti	1a	(0.496 0.496 0.496)
O	3b	(0.479 0.479 0.021)

In the rhombohedral unit cell, a check of the phonon spectrum confirms that a structural energy minimum has been reached, while in the cubic unit cell, three imaginary phonon modes persist.

Next, we multiply the rhombohedral unit cell to obtain a $2 \times 2 \times 2$ supercell. A quick calculation of the phonon spectrum shows that in the large cell, several phonon modes become imaginary. This means that the structure possesses further instabilities at wavevectors commensurate with the $2 \times 2 \times 2$ supercell, e.g. at the X, Y or Z point or along face or room diagonals.

A good way to further relax the structure is to displace the ions along an eigenmode belonging to an imaginary phonon frequency. In the supercell of rhombohedral STO, these remaining imaginary phonon modes correspond exactly to the anti-ferroelectric distorsion. This is also observed in experiment and consistently appears in DFT calculations, regardless of the employed pseudopotential. As was shown in [14], we can conclude that this distorsion is not a computational artefact.

After manually displacing the atoms along the imaginary phonon modes, the structure is again relaxed until convergence is reached.

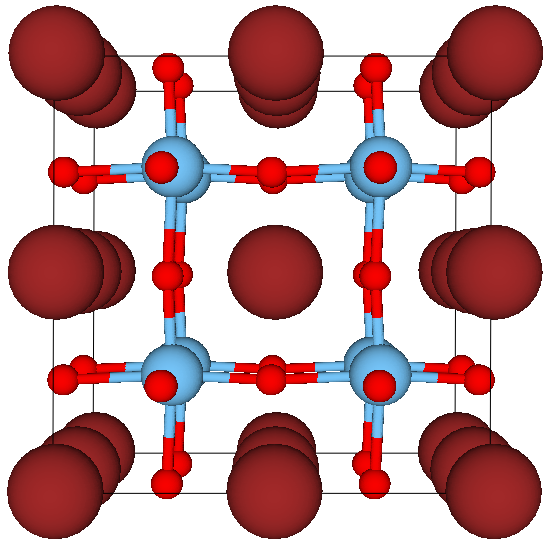

Figure 4.7: rhombohedral $SrTiO_3$ in a $2\times2\times2$ supercell
The central Ti atoms are displaced along the space diagonal, but imaginary phonon modes persist.

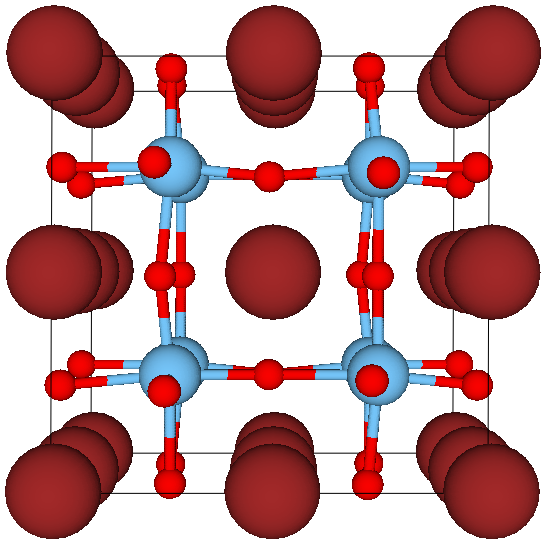

Figure 4.8: rhombohedral $SrTiO_3$ with antiferroelectric distorsion.
Note that neighbouring oxygen cages are rotated in opposite directions around the Ti-O axis.

4.2 Implementation of Kubo-Green

To compute the ionic polarisability from Kubo-Green, we need to implement equation (3.4),

$$\chi_{\alpha\beta}(\omega) = \beta \int_0^\infty \langle \dot{P}_\alpha(0) P_\beta(t) \rangle e^{-i\omega t} dt.$$

We will describe the time-dependent dipole moment $\mathbf{P}(t)$ by the trajectory of the total dipole moment in the unit cell by means of a molecular dynamics simulation (MD). In particular, we want to sample the dipole fluctuations at a predefined temperature. Furthermore, we require a large amount of independent dipole trajectories, as we need to compute a sample average. We will thus follow the following procedure:

1. Initialise independent starting configurations We select the initial configuration (cubic or rhombohedral phase) depending on the temperature at which we want to simulate the dipole flucutations. For a simulation below the first phase transition, we initialise the system in the rhombohedral phase, while for simulations at high temperature, we start from the configuration in the cubic phase.

For the systems and the temperature range that interest us, decorrelation times in an MD simulation are very long. One way to obtain independent samples of the dipole moment is to start a very long NVT run, estimate the decorrelation time of the system and pick intermediate structures from the NVT run at sufficiently large intervals. However, since this approach takes a lot of computing time, we will rather use a different routine implemented in VASP.

In VASP, it is possible to create a sample of configurations of a given system whose total energy follows the Maxwell-Boltzmann distribution of kinetic energies in a thermodynamic system at temperature T. This is done using the PHON_LMC routine. This routine assigns, on average, a kinetic energy of $k_BT/2$ to each quadratic degree of freedom in the system. The

motion of the atoms is restricted to the specific displacement vector determined by the eigenmode of the system. Note, that the kinetic energy is sample from a classical distribution function.

At first, phonon modes and phonon eigenfrequencies of the whole system are computed. Then, for each ion individually, the routine draws a random configuration from the density matrix of a classical harmonic oscillator in a canonical ensemble at temperature T and assigns it to the ion. Thus we create a configuration where each ion is displaced along the eigenmode and the magnitude of the displacement is commensurate with the temperature of the entire system. This way, we can make sure to produce fully independent initial structures for the MD run.

2. Equilibration in a canonical ensemble Follwing the initialisation, we run an MD simulation in VASP with an Andersen thermostat to fully equilibrate the system at temperature T. This is required, since the initialisation described above relies on the harmonic approximation, i.e., it only accounts for the quadratic terms in the potential energy surface.

The unit time step of the MD is 1 femtosecond and the usual runtime is 2,000 to 10,000 steps. In every step, VASP computes the configuration energy and inter-ionic forces for the following timestep.

In a microcanonical ensemble (NVE ensemble), only interatomic forces are taken into account. In a canonical ensemble, however, one also needs to simulate the external heat bath, which alters the phase space of admissible microstates. Using the Andersen thermostat, the contact with the heat bath is simulated by resetting the kinetic energy of a randomly selected particle to a value drawn from a Maxwell-Boltzmann distribution at temperature T. This resetting should not occur too frequently in order not to interfere with the internal dynamics of the system.

Observation of the temperature fluctuations helps to assess whether the considered system has reached thermal equilibrium. For STO and BTO, this was usually reached already after several hundred timesteps.

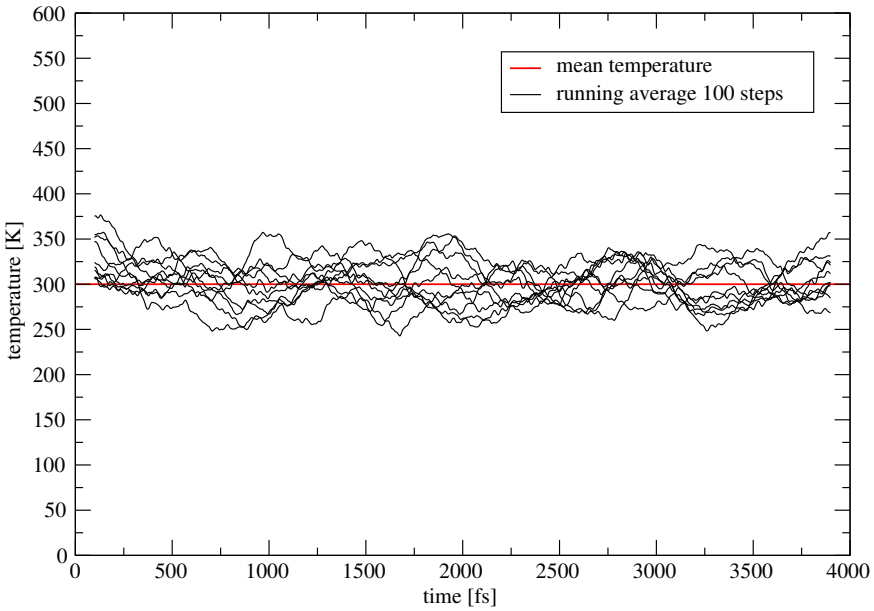

Figure 4.9: Thermal equilibration of 10 independent $BaTiO_3$ systems in the cubic $2 \times 2 \times 2$ supercell using an Andersen thermostat at 300 K. This simulation was erroneously initialised using Bose-Einstein statistics. During the classical MD simulation, the initial temperature turns out to be slightly too high, however, the Andersen thermostat quickly equilibrates the system properly.

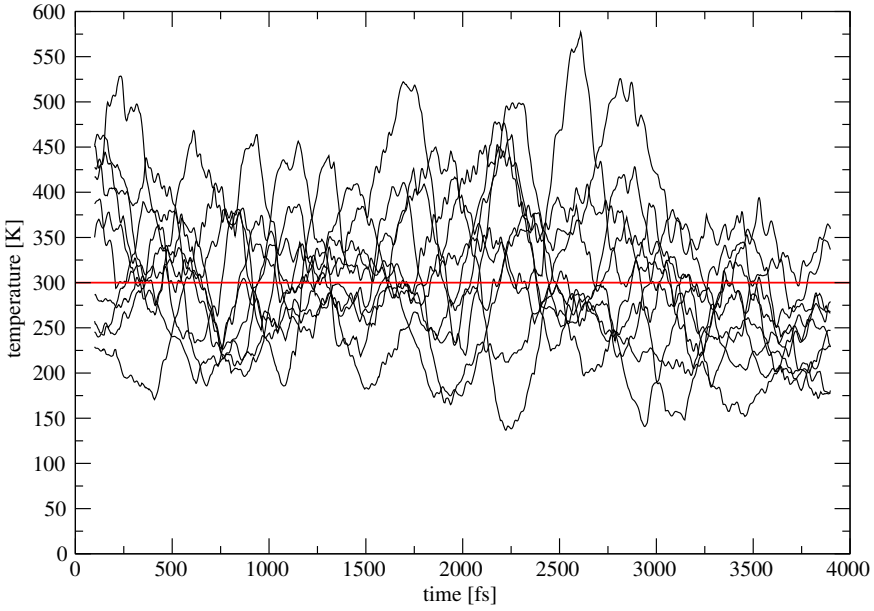

Figure 4.10: Thermal equilibration of 10 independent $SrTiO_3$ systems in the cubic unit cell using an Andersen thermostat at 300 K

Note that the system in the supercell consists of 40 atoms, while the system in the unit cell only has 8 atoms. Thermal fluctuations in a system of N particles are proportional to $1/\sqrt{N}$, which explains why the fluctuations in the unit cell are so much larger than in the larger supercell. In fact, the ratio between the size of the fluctuation should be approximately $\sqrt{40/8} = \sqrt{5} \approx 2.236$.

3. Dipole time-autocorrelation in the NVE ensemble On average, the final structures of the equilibration in the NVT run should represent the canonical ensemble at temperature T. In the last step, we compute a trajectory for the total dipole moment of the material for every individual system in the sample.

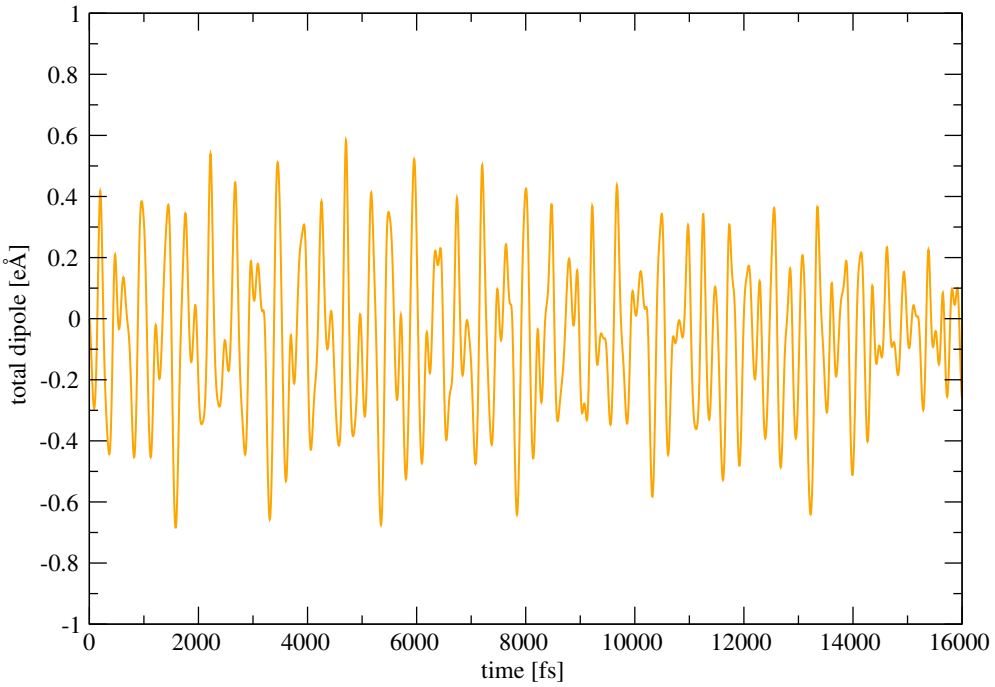

Figure 4.11: Trajectory of the total dipole of SiO_2 at 100 K. The dipole moment, set to zero initially, is given in units of elementary charge times Angstrom

First, the Born effective charges are computed in the unit cell. Then, the MD simulation in a microcanonical ensemble is started. The displacements of the ions at each step are stored. The change of the dipole over the runtime is simply given by the multiplication of the change of the ionic positions times the Born effective charges (cf. equation 3.23).

Note that the initial dipole is, somewhat arbitrarily, set to zero. The concept of Born effective charges can only be employed when the dipole changes as a result of a change of ionic positions. We cannot obtain a value for the initial total dipole from the Born effective charges. However, as discussed in section 3.1.2, there is a very simple connection between the response function and its time derivative. Since by taking the derivative with respect to time, the constant offset of the dipole vanishes, and we can compute the response function using equation (3.7).

Also, it is important to note that the runtime and timestep for the NVE run must be chosen such that a good resolution of the resonance frequencies can be achieved. From the theory of Fourier transformation we know that we can only resolve frequencies that lie between the inverse of the total runtime (lower bound) and the inverse of twice the length of the timestep (upper bound).

Having obtained a sufficiently large set of dipole trajectories, we should be able to implement equation (3.4). However, there is one last complication: Since we do not know the initial value of the total dipole, we have to take a small detour and compute the time-derivative $\dot{\mathbf{P}}(t)$ of the dipole $\mathbf{P}(t)$. Thusly, we get rid of the constant offset of the initial position, and we can simply use the expression we previously derived for the electric conductivity,

$$\chi^{\rho\mathbf{j}}_{\alpha\beta}(\omega) = \sigma_{\alpha\beta}(\omega) = \beta \int_0^\infty \langle \dot{P}_\alpha(0)\dot{P}_\beta(t)\rangle e^{-i\omega t} dt, \tag{3.7}$$

and recover (3.4) via the identity

$$\chi^{\rho\rho}_{\alpha\beta}(\omega) = \frac{1}{i\omega}\chi^{\rho\mathbf{j}}_{\alpha\beta}(\omega). \tag{3.9}$$

We compute the time-derivative of the dipole moment using central differences, compute the autocorrelation function $\dot{\mathbf{P}}(0)\dot{\mathbf{P}}(t)$ and average over all samples of the ensemble by computing the mean value. This quantity is then Fourier transformed and scaled by β.

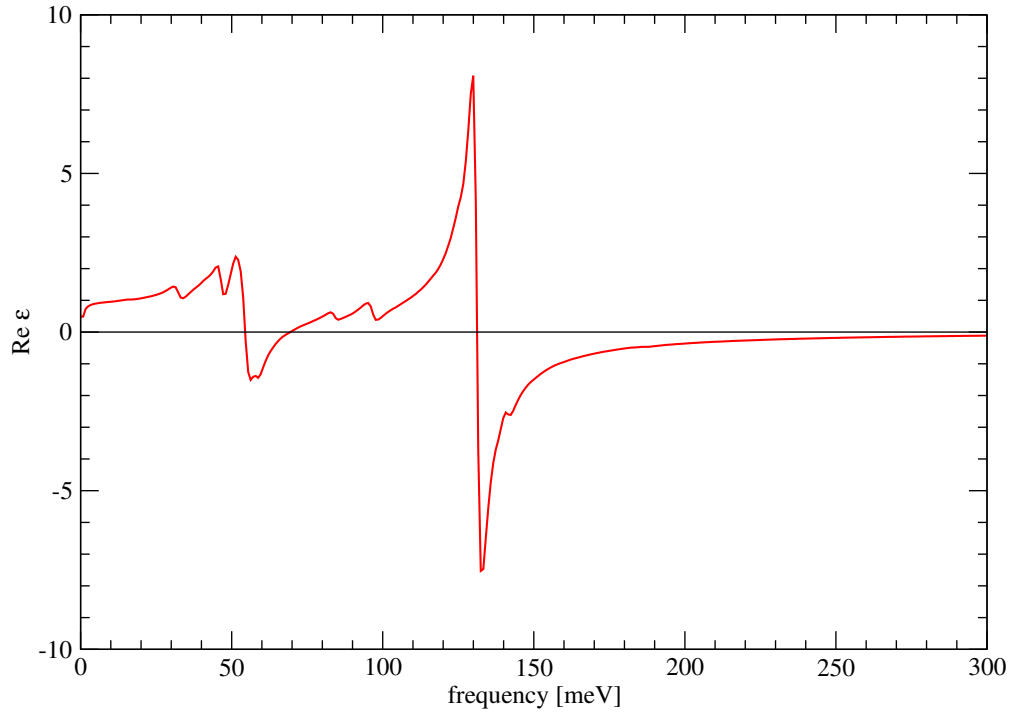

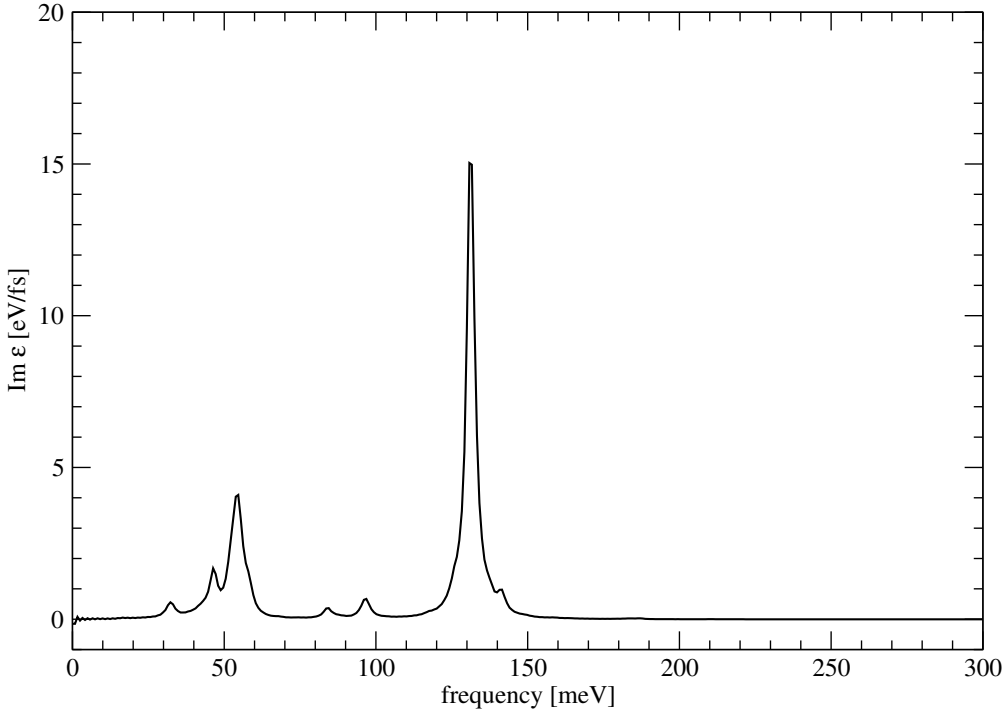

Figure 4.12: Damped Fourier transform of the single dipole trajectory of SiO_2 at 100 K from figure 4.11.

4.3 Implementation of the delta pulse method

The implementation of the Delta pulse method requires less computing time, but is only applicable to very low temperatures. Furtermore, depending on the system, we found it more difficult to apply, often necessiting a careful evaluation of a large number of parameters, so that many MD runs were needed to obtain satisfactory results.

We start again from the relaxed ground-state configuration and start a molecular dynamics simulation. In the very first time step, we apply a (small) electric field across the unit cell, which excites all dipole-active phonon modes. Using the same procedure as above, we keep track of the total dipole moment of the unit cell over time, and compute its Fourier transformation.

As we have seen in section 3.2, it may be necessary to eliminate contributions from a non-zero initial dipole moment. This is achieved by applying the electric field once in positive and once in negative direction, and then by subtracting the response obtained from the pulse in negative direction from the one obtained from the one in positive direction.

According to equation (3.13), the actual field strength applied in the first MD step should have no influence on the outcome of the frequency-dependent polarisability, as in the formula for the response function, we divide out the dependence on the field strength. However, since the formula we derived is only correct for the description of linear response, it is only those contributions that are not affected by the strength of the electric field.

Depending on the system, there may be significant anharmonic effects which can be amplified by an increasing size of the perturbation. Strong anharmonic effects can in fact spoil the signal of the dipole moment, as can be seen at the example of SiO_2 in figure 4.13. The larger the applied electric field, the more pronounced the artefacts at certain frequencies become.

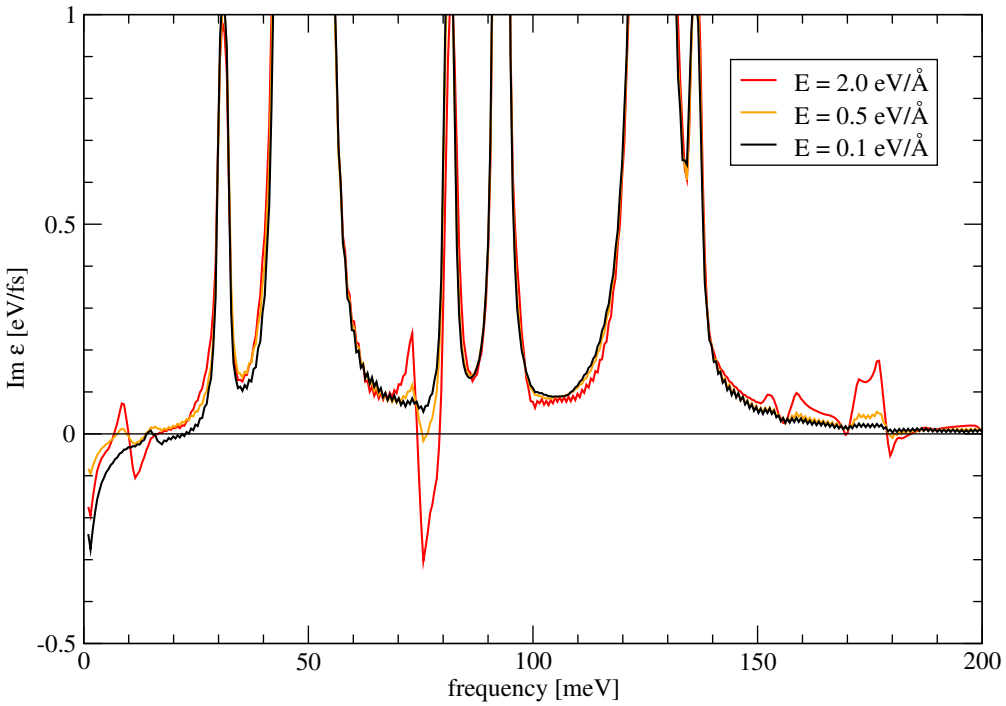

Figure 4.13: Detail of the imaginary dielectric function of SiO_2 at 100 K. Artefacts around 10 meV, 75 meV and above 150 meV can at least in part be explained by anharmonic effects as a consequence of a large external electric field.

Before employing the delta pulse method, it is important to test the convergence of the results with respect to the applied field to make sure that on the one hand, the signal of the dipole moment is visible, but also that on the other hand, anharmonic effects do not cause too much noise in the signal.

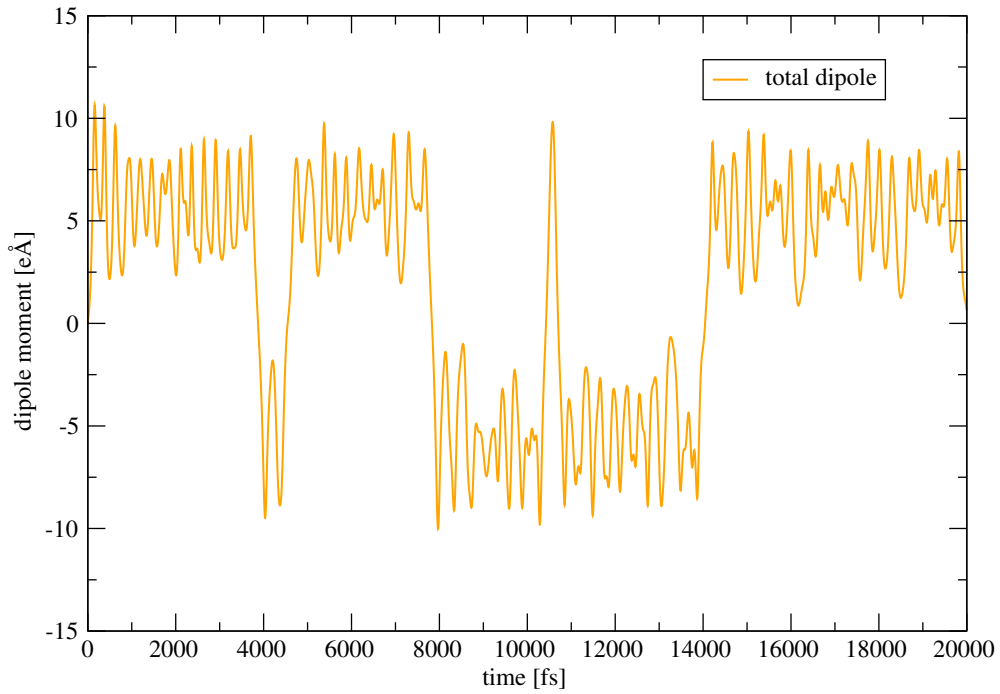

Figure 4.14: Trajectory of the dipole moment of cubic $BaTiO_3$.

An extreme case, in which anharmonic effects spoil the simulation of the linear response, are structurally unstable systems, or such systems which are very close to a structural instability. If we apply only a small electric pulse to a system like cubic $BaTiO_3$, whose dynamical matrix is not positive definite, we can cause the entire system to move into a new local energy minimum. The resulting dipole trajectory is shown in figure 4.14.

Often, these local energy minima will be lower in energy, but some may also have a slightly higher potential energy. These problems can also appear in a system whose dynamical matrix is positive definite, but whose structures exhibits many local energy minima in the neighbourhood of the global miminum. If the system moves to a new energy minimum, the evaluation of the polarisability becomes virtually impossible. It is instructive to take a look at the dipole trajectory, to understand why this causes problems.

Even though the applied electric field in figure 4.14 was very small, the large jumps in the dipole trajectory hint at the occurrence of phase transitions in the course of the simulation. While it is still possible to obtain good results for cubic $BaTiO_3$ from Kubo-Green, the delta-pulse method is limited to dynamically stable systems. The Fourier-transformed signal from figure 4.14 does not show any discernible pattern.

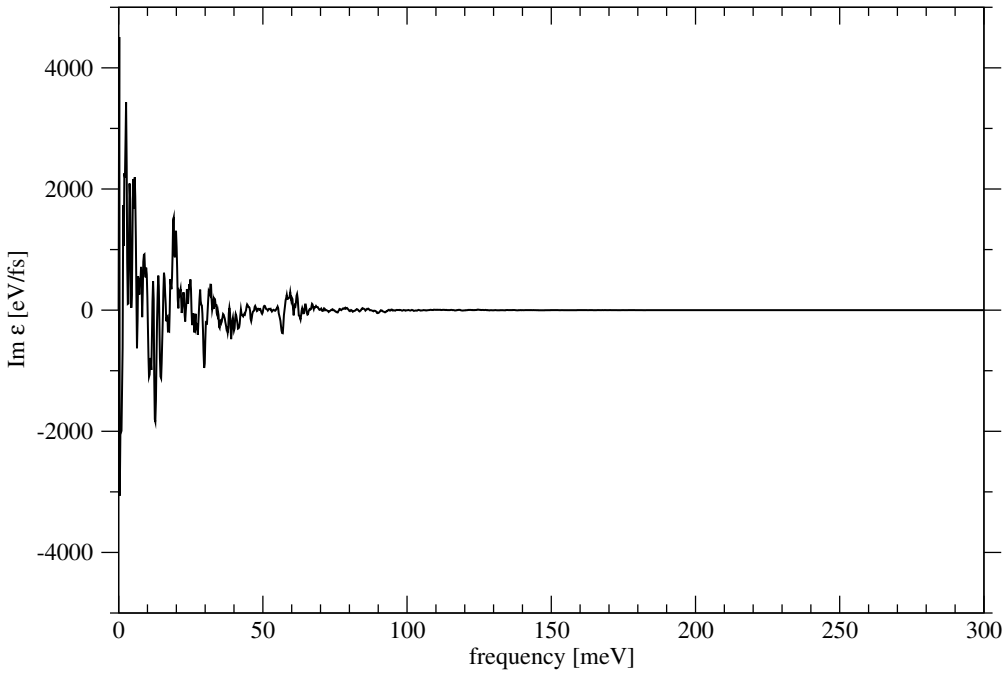

Figure 4.15: Fourier-transformed dipole moment of cubic $BaTiO_3$

Chapter 5

Results and Discussion

5.1 First application and testing: SiO_2

First, we compare the Kubo-Green result for the ionic polarisation with the standard method using the phonon spectrum. As SiO_2 is stable up to high temperatures, the Kubo run was performed at 100 K. The selected timestep was 2.0 femtoseconds and the total runtime was 5000 femtoseconds. The resulting dielectric function is shown below.

Remember that the dielectric function is in general a tensorial quantity. Since α-quartz has a three-fold rotation symmetry around the z-axis, the xx-component is the same as the yy-component of the dielectric tensor. The broadening of the peaks in the Kubo-Green method decreases with the length of the total simulation time, and increases with the temperature. The increase with temperature is a real physical effect, caused by phonon-phonon scattering which decreases the lifetime of harmonic states.

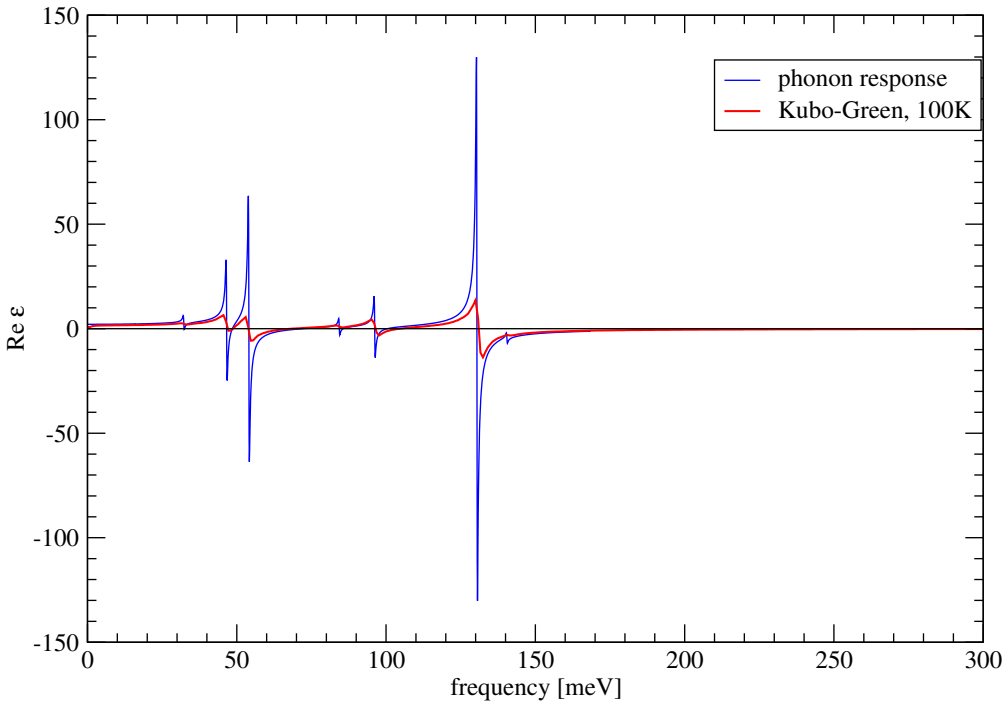

Figure 5.1: Real part of the xx-component of the dielectric tensor of α-SiO_2.

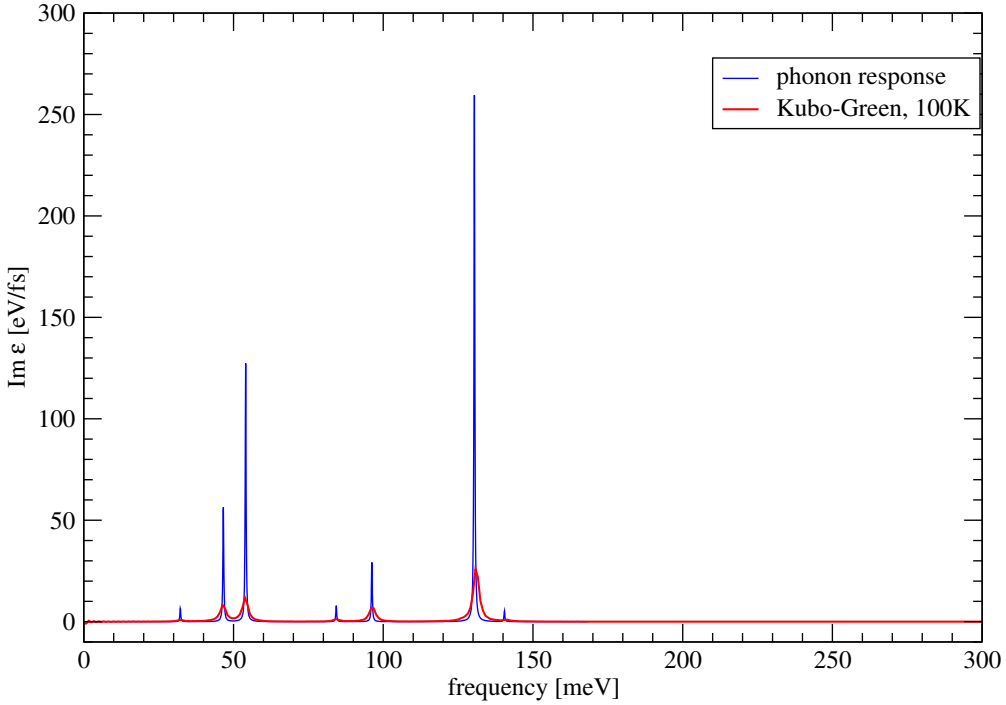

Figure 5.2: Imaginary part of the xx-component of the dielectric tensor of α-SiO_2.

A necessary condition for accurate results in both the Kubo-Green and the delta pulse approach is energy conservation during the MD simulation. As the trajectory of the dipole is always computed in a microcanonical ensemble, we expect the total energy of the system to be conserved throughout the simulation. In all our simulations, energy conservation was satisfying. Throughout the Kubo-Green run for SiO_2, the total, potential and kinetic energies yielded the results given below.

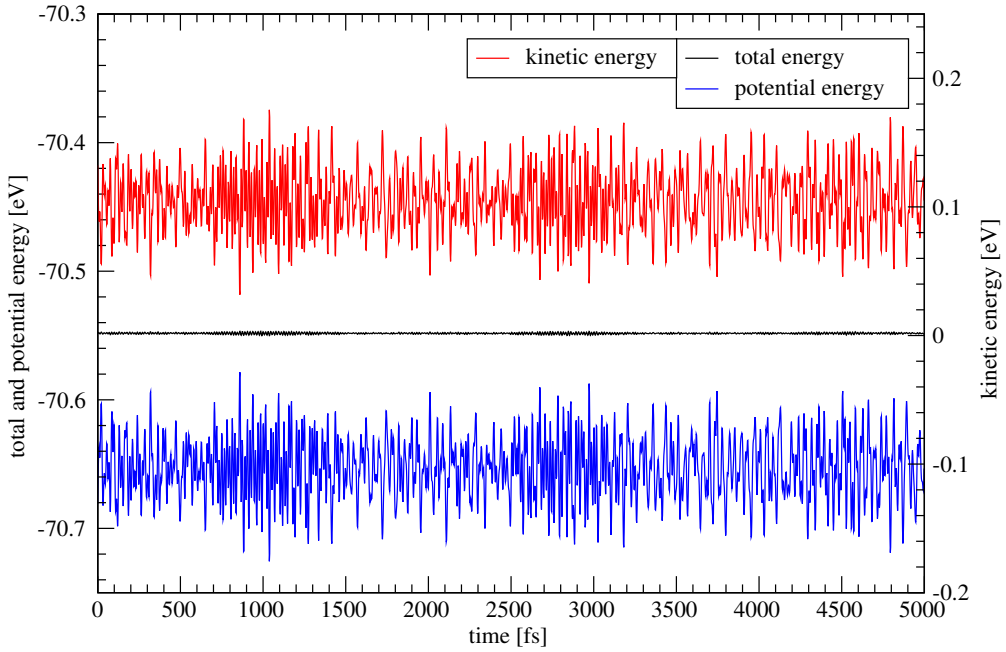

Figure 5.3: Total, potential and kinetic energy of SiO_2 throughout the molecular dynamics simulation; note the different energy axes for total and potential as well as kinetic energy

The net energy drift in figure 5.3 is of the order of 1.5 meV. According to the equipartition theorem, we have

$$E_{kin} = \frac{f}{2} k_B T,$$

where f is the number of degrees of freedom in the system. In a system of 9 atoms, we have 27 position coordinates, of which three are translational and therefore do not contribute to the thermal energy. If we distribute the kinetic energy equally among the remaining 24 degrees of freedom, we can estimate the energy loss to be equivalent to a thermal energy of about 0.7 K. Compared to the 100 K at which the simulation was run, this amount of thermal energy seems negligible.

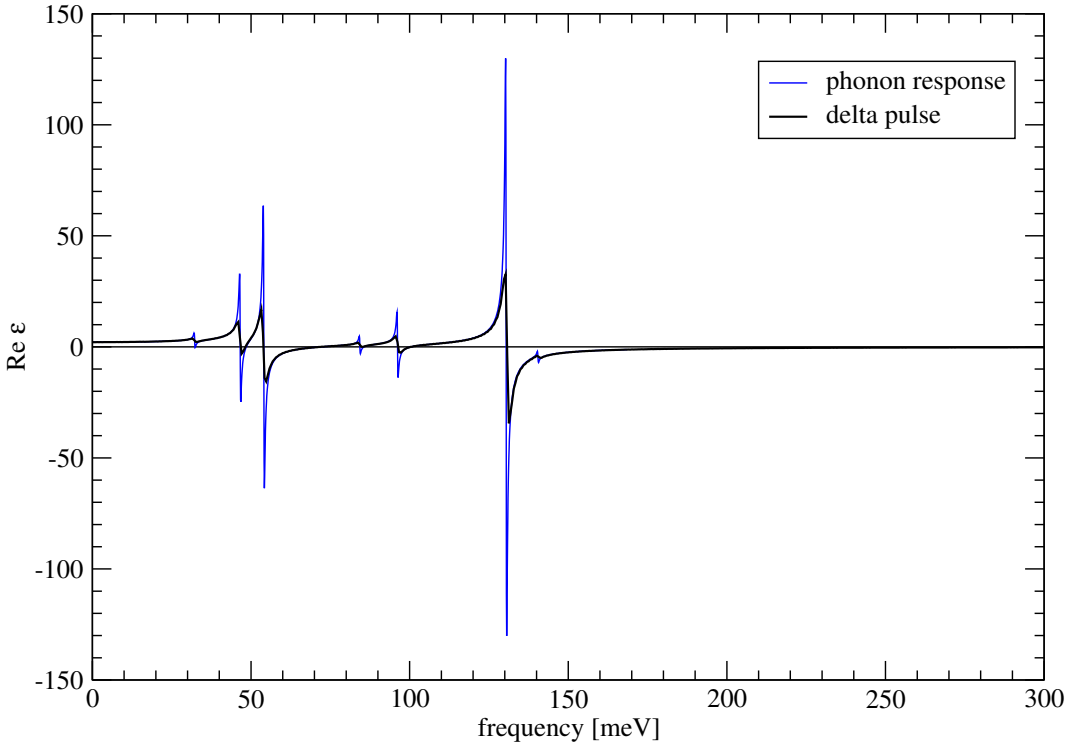

Figure 5.4: Real part of the xx-component of the dielectric tensor of α-SiO_2.

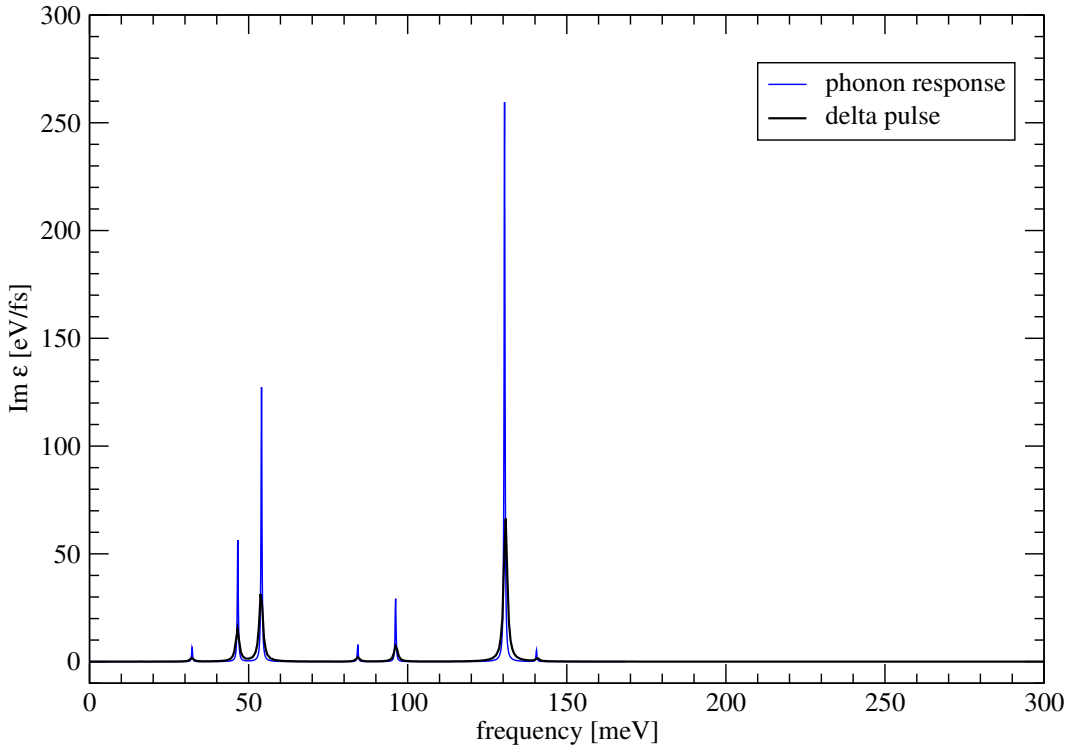

Figure 5.5: Imaginary part of the xx-component of the dielectric tensor of α-SiO_2.

Next, we consider the results of the delta pulse method for SiO_2. The polarisability functions shown in figures 5.4 and 5.5 were obtained from a run of 4000 fs with a timestep of 1 fs.

Again, we check energy conservation during the MD in the microcanonical ensemble. We registered the following behaviour.

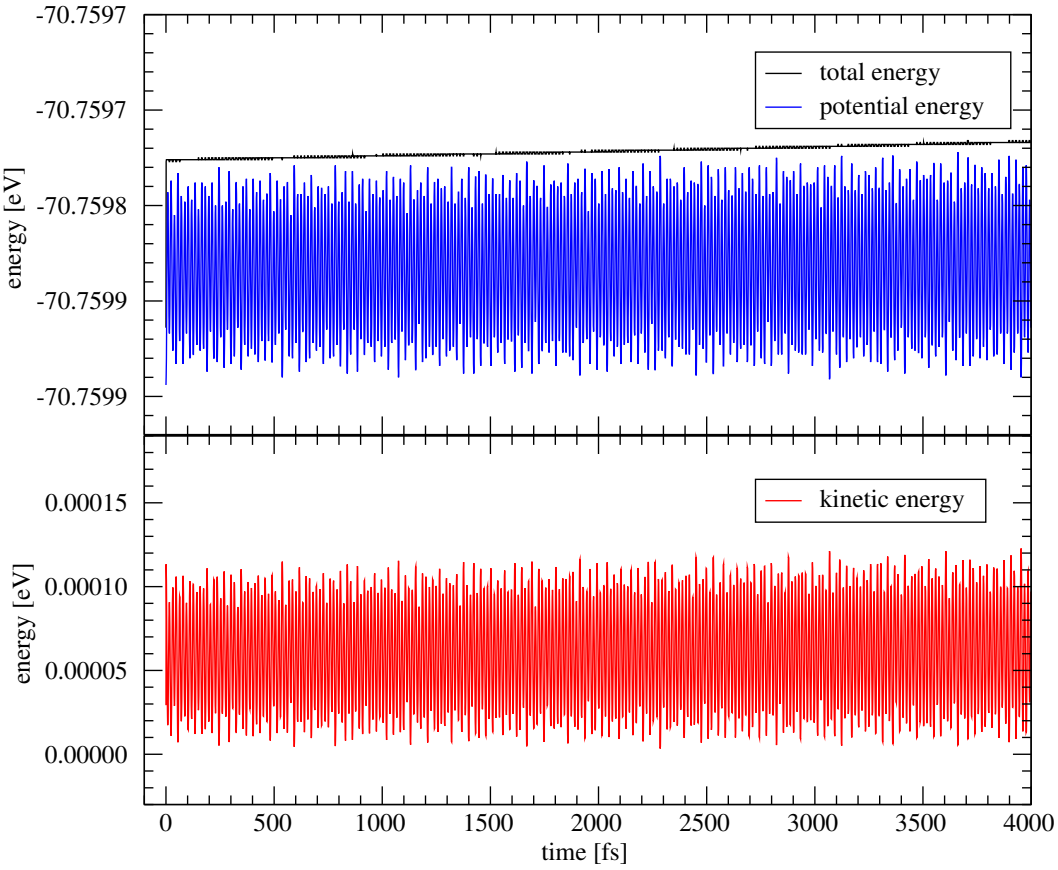

Figure 5.6: total, potential and kinetic energy of SiO_2; note the initial jump in the total energy due to the applied delta pulse

Note that the average kinetic energy observed in the simulation following the delta pulse is smaller by a factor of almost three orders of magnitude. Indeed, the delta pulse simulation ran at a temperature of only around 0.1 K. This also explains, why the absolute values of the energy fluctuations observed in the delta pulse method are several orders of magnitude smaller than those in the Kubo-Green simulation.

The energy drift in figure 5.4 is smaller than 0.01 meV, which means a loss of thermal energy of less than 0.05 K. An energy drift of this magnitude may in fact not be negligible any more, however, the results were still satisfactory.
On the basis of figures 5.1 to 5.4, we can confirm that both methods, the Kubo-Green relation and the delta pulse method, can indeed yield reliable results for the polarisability of a material. After this rather simple and very stable system, we will now move on to applying the same procedure to the more interesting cases of $BaTiO_3$ and $SrTiO_3$.

5.2 Barium titanate: ionic response

We begin with the low-temperature phase of $BaTiO_3$, the rhombohedral structure in the simple unit cell. To investigate the polarisability close to the absolute zero, we first compare the delta pulse and phonon response methods.

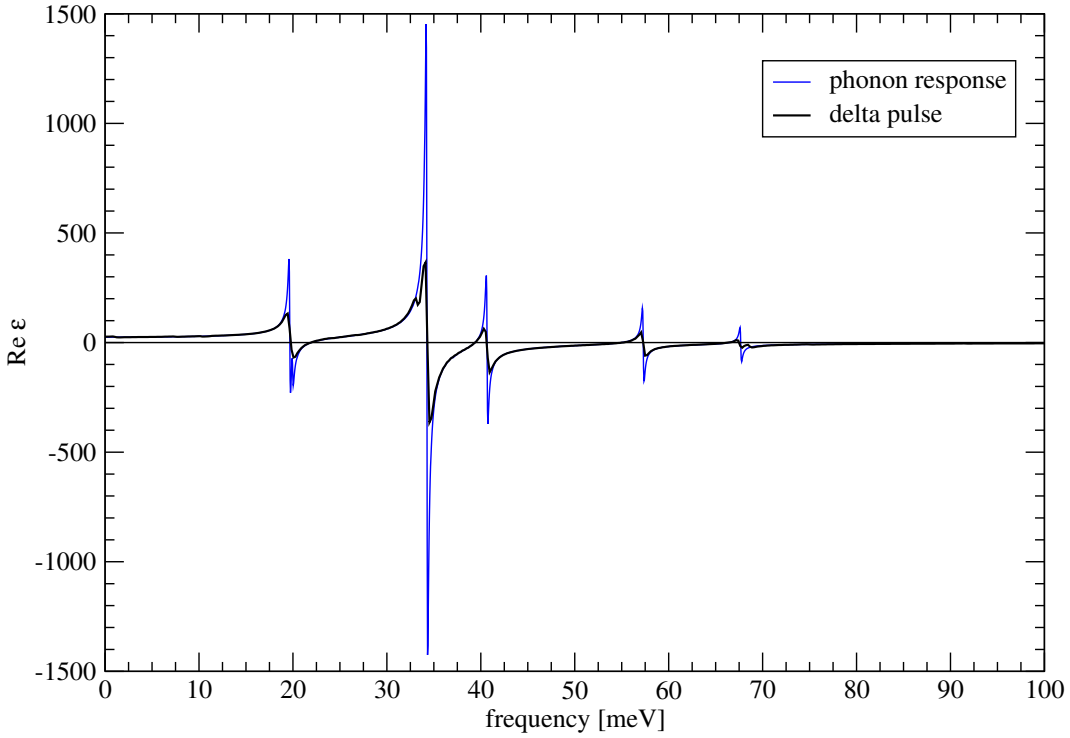

Figure 5.7: Real part of the xx-component of the dielectric tensor of rhombohedral $BaTiO_3$ at very low temperature

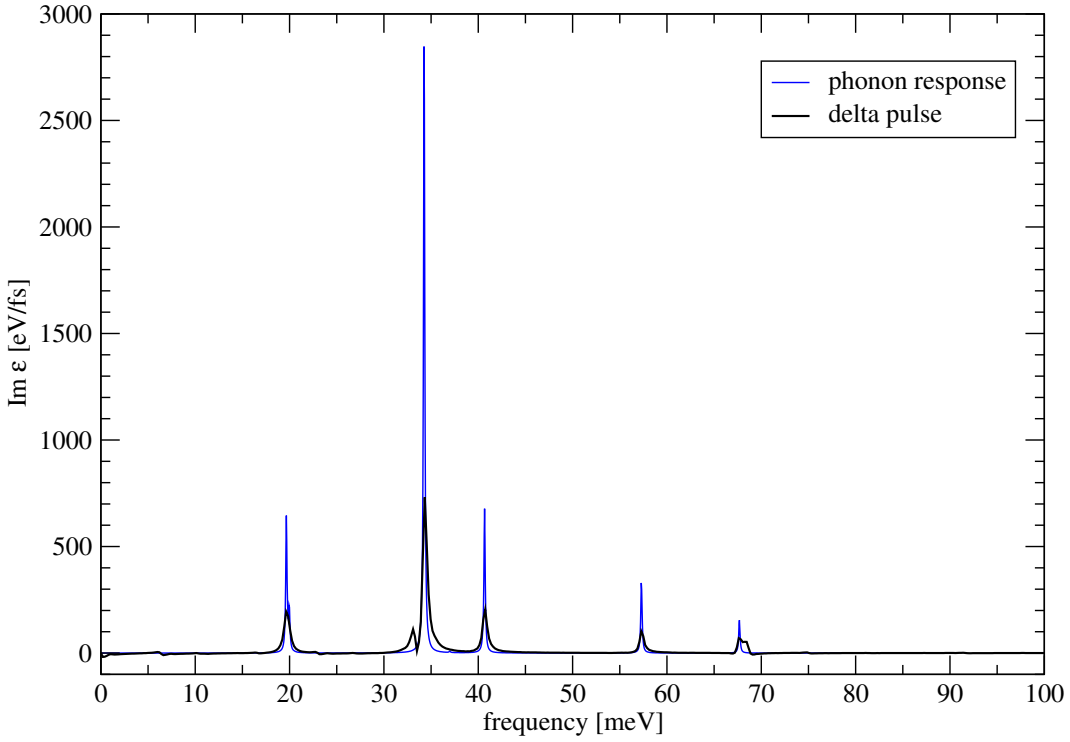

Figure 5.8: Imaginary part of the xx-component of the dielectric tensor of rhombohedral $BaTiO_3$ at very low temperature.

For the fully-relaxed rhombohedral barium titanate, the delta pulse and phonon response methods give largely identical results. However, further investigation of the question why the delta pulse method exhibits two extra peaks at 33 meV and 68 meV is required. Also, note that the modes involved in the polarisability of barium titanate are by a factor 10 more dipole active than in SiO_2.

Again, energy conservation is reasonably good for the delta pulse method. In the following graph, we show the total, potential and kinetic energy from the first of the two delta pulse runs; the pattern in the second run is very similar.

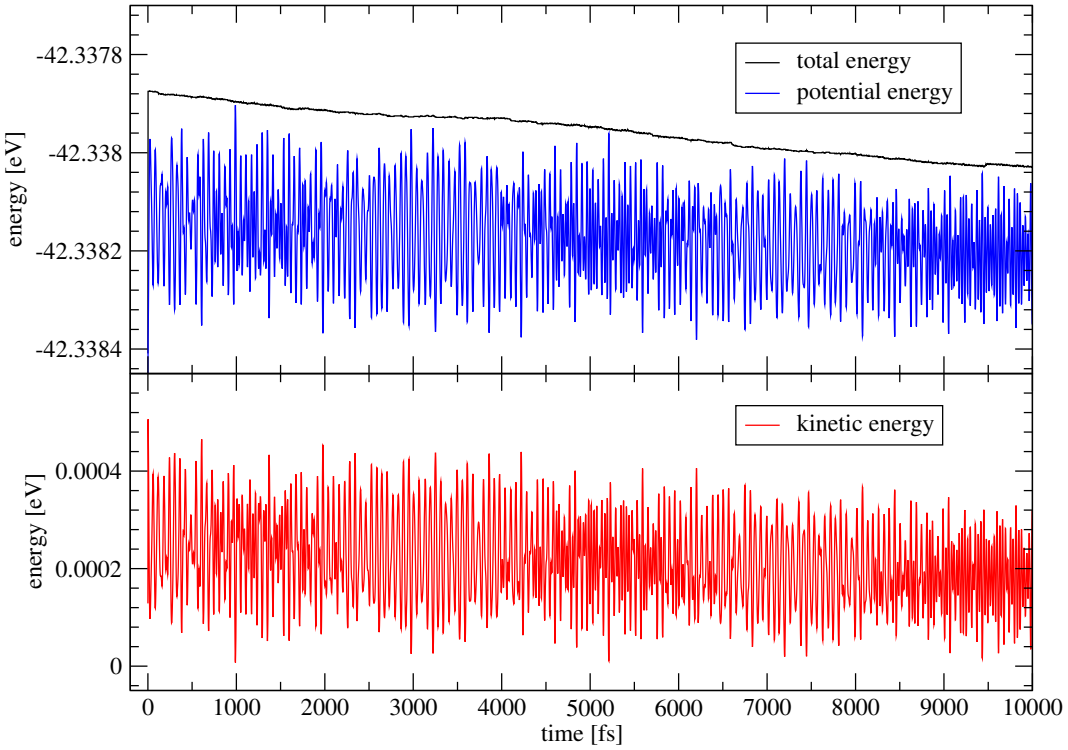

Figure 5.9: Total, potential and kinetic energy of rhombohedral $BaTiO_3$ at low temperature.

Note again the energy axis. The shift of the total energy is less than 0.16 meV. In a system of five atoms, this is the equivalent of about 1.9 Kelvin. Compared to the total temperature of about 5 Kelvin, this energy drift may not be negligible anymore. However, the total results are still satisfactory.

Next, we compare the results from the Kubo-Green relation for the dielectric function at low temperatures to the phonon response. We run two Kubo-Green simulations, one at 10 K and one at 50 K, both far below the temperature of the first phase transition, and compare the results to the phonon response.

The positions of the individual peaks mostly agrees with the linear-response approach. This is particularly true at the lower temperature of T=10 K, while at T=50 K, a significant broadening of the peaks is observed. This indicates very strong anharmonicities in $BaTiO_3$, leading to a sigificant reduction of the life time of the phonon modes.

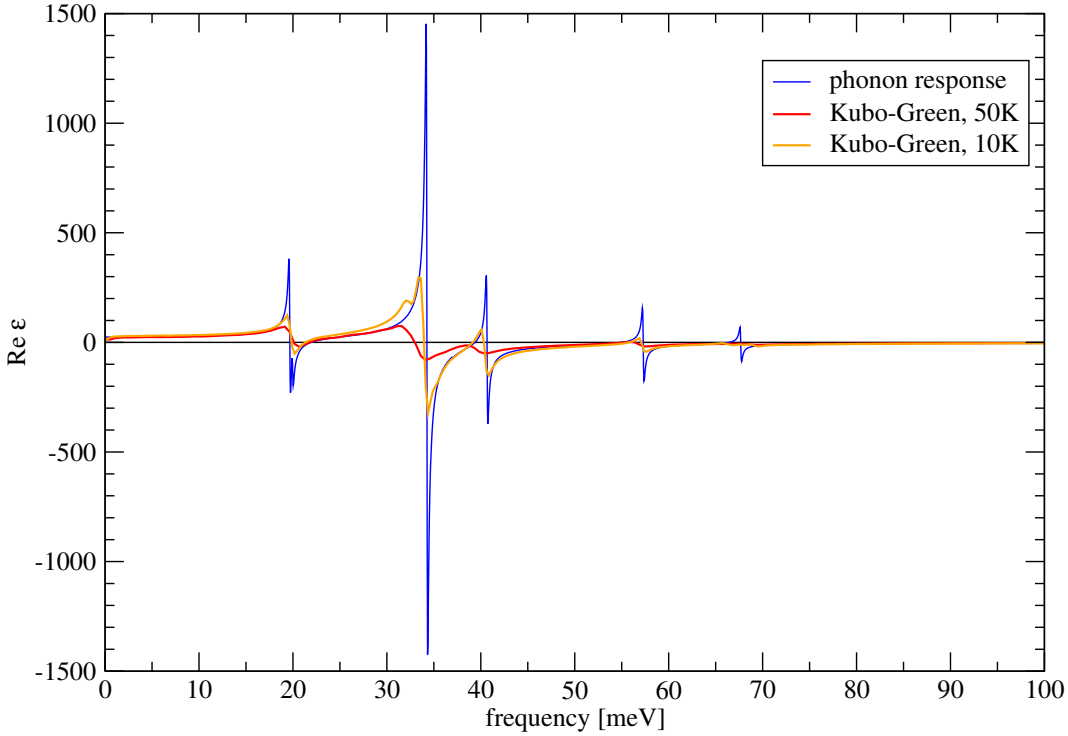

Figure 5.10: Real part of the xx-component of the dielectric tensor of rhombohedral $BaTiO_3$ at low temperature.

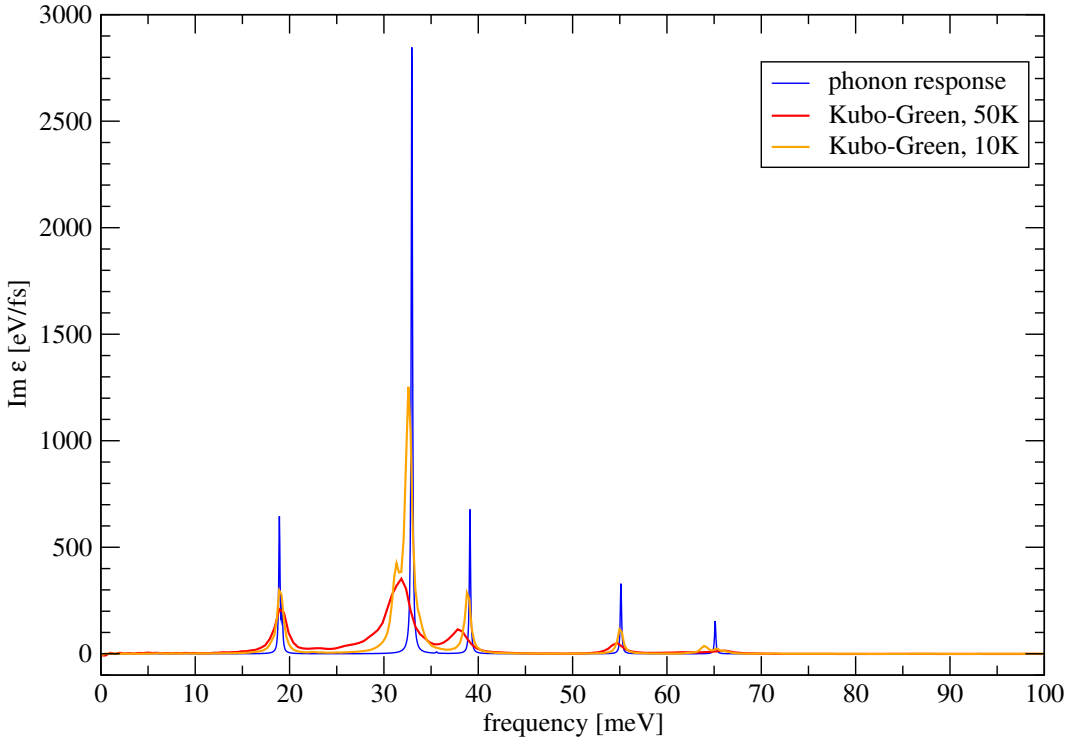

Figure 5.11: Imaginary part of the xx-component of the dielectric tensor of rhombohedral $BaTiO_3$ at low temperature.

This is in fact quite remarkable, since the simulation temperatures are still far below the transition temperatures to the next higher symmetry structure. Already at T=10 K, the peak at 34 meV shows a shoulder at 32 meV. This shoulder was also present in the delta-peak simulations, but less pronounced. Clearly, this is the first mode to be affected by anharmonic effects. At T=50 K, the spectrum is again fairly smooth, but the peaks are shifted to lower frequencies by about 10% compared to the phonon response.

Lastly, let us turn to the high-temperature behaviour of $BaTiO_3$. In the figure below, we compare the results of the Kubo-Green polarisability for barium titanate in the simple unit cell with the results obtained in the $2 \times 2 \times 2$ supercell.

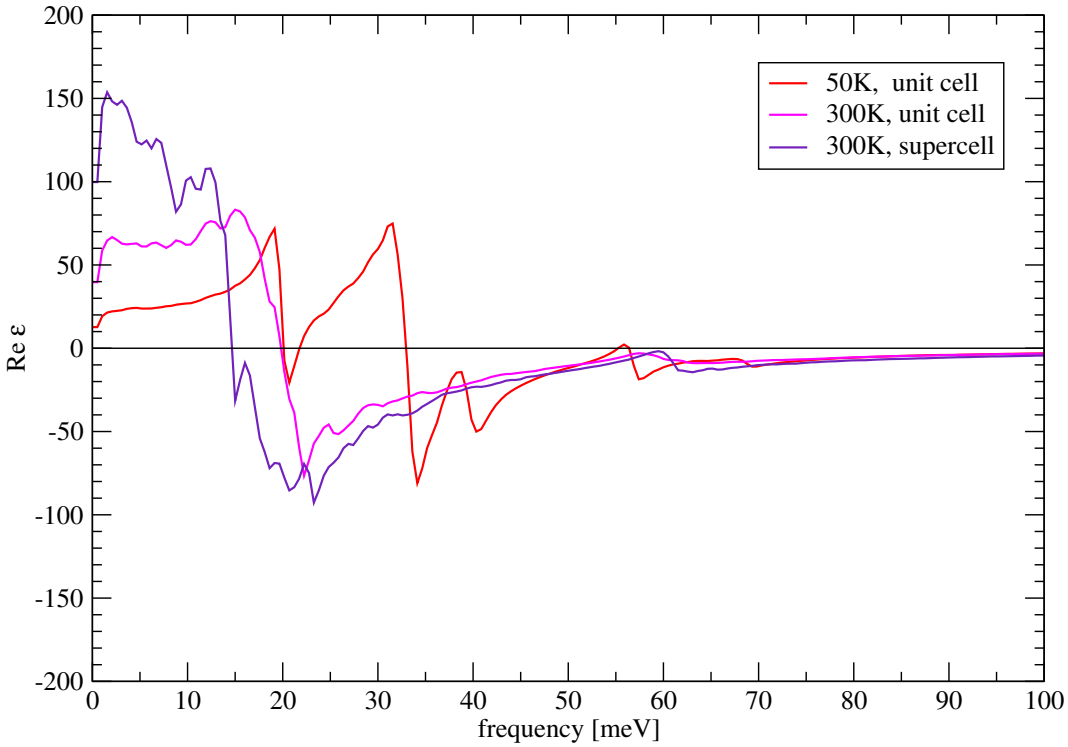

Figure 5.12: Real part of the low- and high-temperature dielectric functions of cubic $BaTiO_3$ as obtained from Kubo-Green

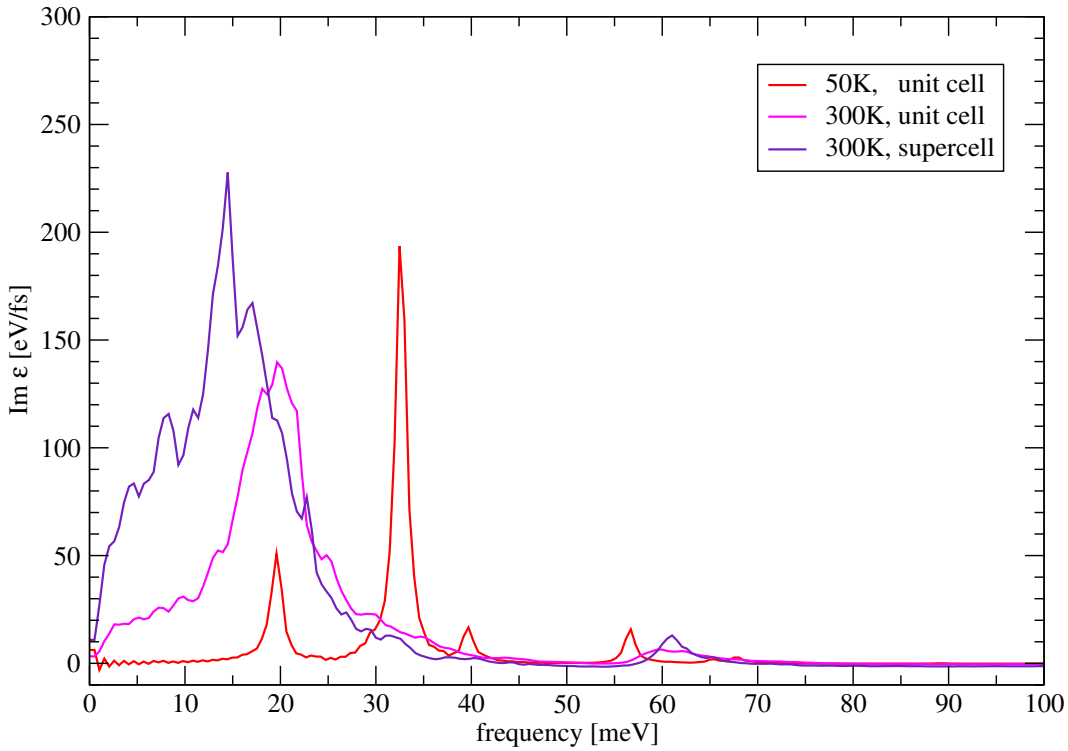

Figure 5.13: Imaginary part of the low- and high-temperature dielectric functions of cubic $BaTiO_3$ as obtained from Kubo-Green.

Both curves are converged with respect to the total runtime. However, the observed difference between the two curves hints at the fact that a simple unit cell is not large enough to provide a comprehensive description of the dielectric properties of the material in the rhombohedral phase.

In the supercell, we observe stronger resonance at lower frequency, which hints at the existence of very soft modes which are only accessible in a supercell. We believe that these are related to the clockwise and counter-clockwise rotations which were discussed in figure 4.6. As mentioned in the introduction, these anti-ferroelectric modes are stable in $BaTiO_3$, but fluctuations along these modes are still possible. However, since these modes are anti-ferroelectric, their net dipole is - in principle - zero. This means that they can only couple to an external field via strong anharmonic effects.

Note that we did not compare the results to the phonon response. This is because the dynamical matrix of cubic $BaTiO_3$ is not positive definite. This can lead to imaginary contributions to the ionic polarisability. Since it is unclear how one should treat these contributions, the only reasonable way to describe the high-temperature polarisability of such systems is by means of a Kubo-Green relation.

Again, the total energy was conserved in all considered the MD simulations. In figure 5.14, we present the total energy of the MD simulation of cubic $BaTiO_3$ in the supercell at 300 Kelvin.

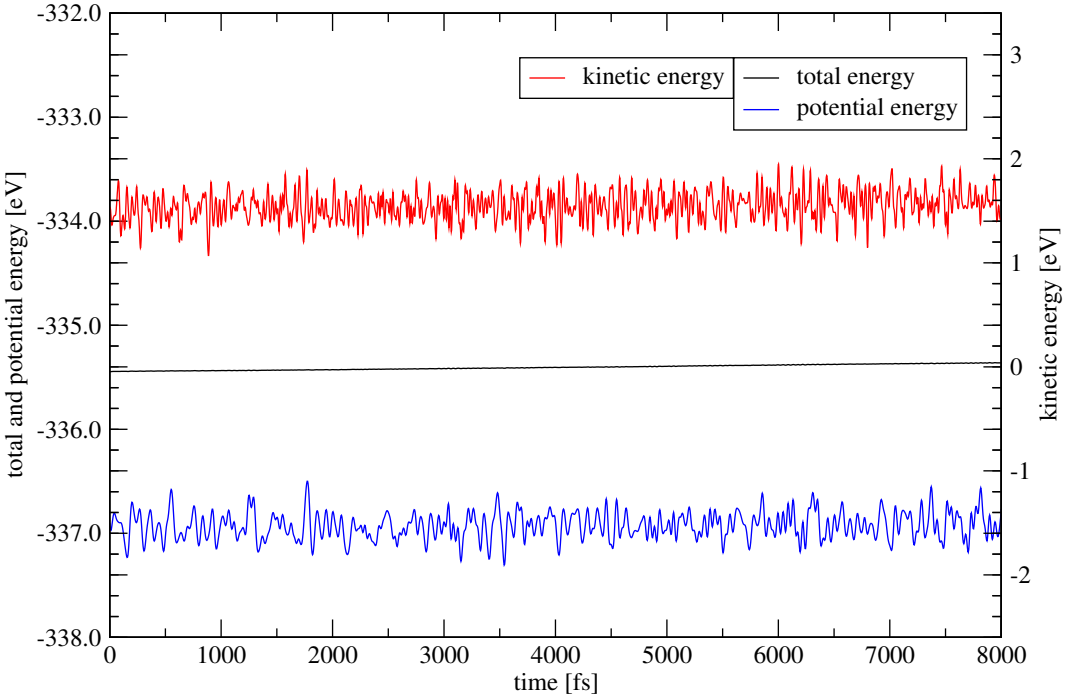

Figure 5.14: energy conservation in cubic $BaTiO_2$ in a $2 \times 2 \times 2$ supercell

The total energy drift amounts to 171.5 meV, which is the equivalent of around 35K. This appears to be satisfactory again.

5.3 Strontium titanate: ionic response

Eventually, we turn to the most complicated and unstable of our test systems, strontium titanate (STO). First, we look at the rhombohedral structure of STO at T=0K and compare the results obtained from the delta pulse and the phonon response. The delta pulse simulation was run with a stepsize of 2.0 fs and a total runtime of 10,000 femtoseconds.

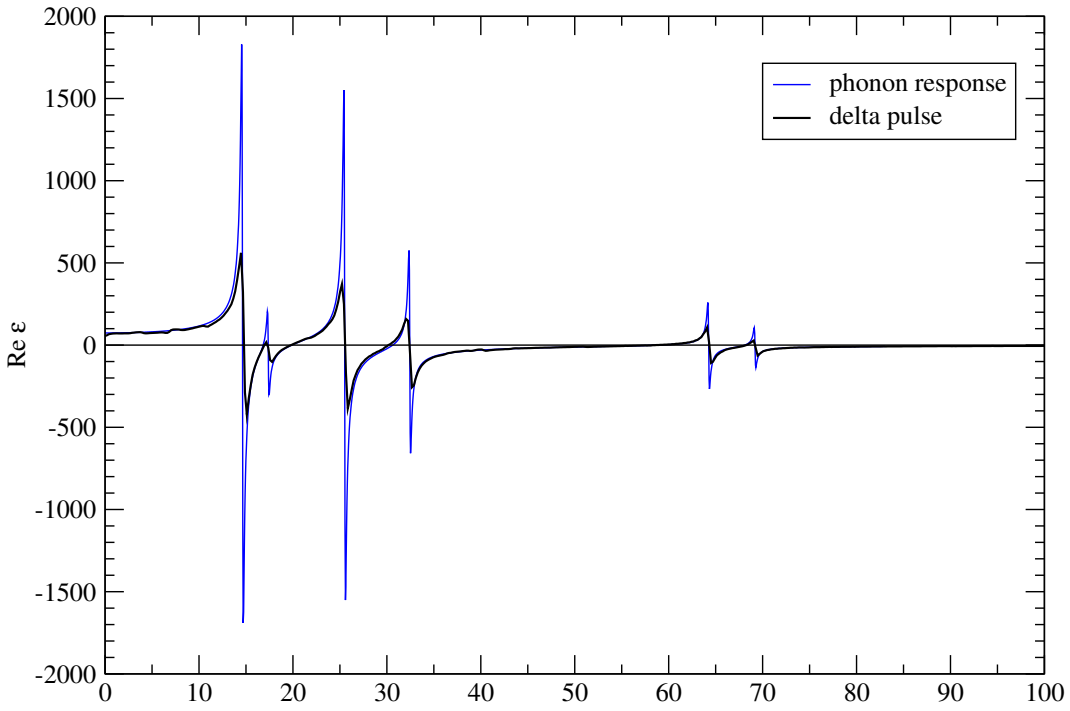

Figure 5.15: Real part of the xx-component of the dielectric tensor of rhombohedral $SrTiO_3$ at low temperature.

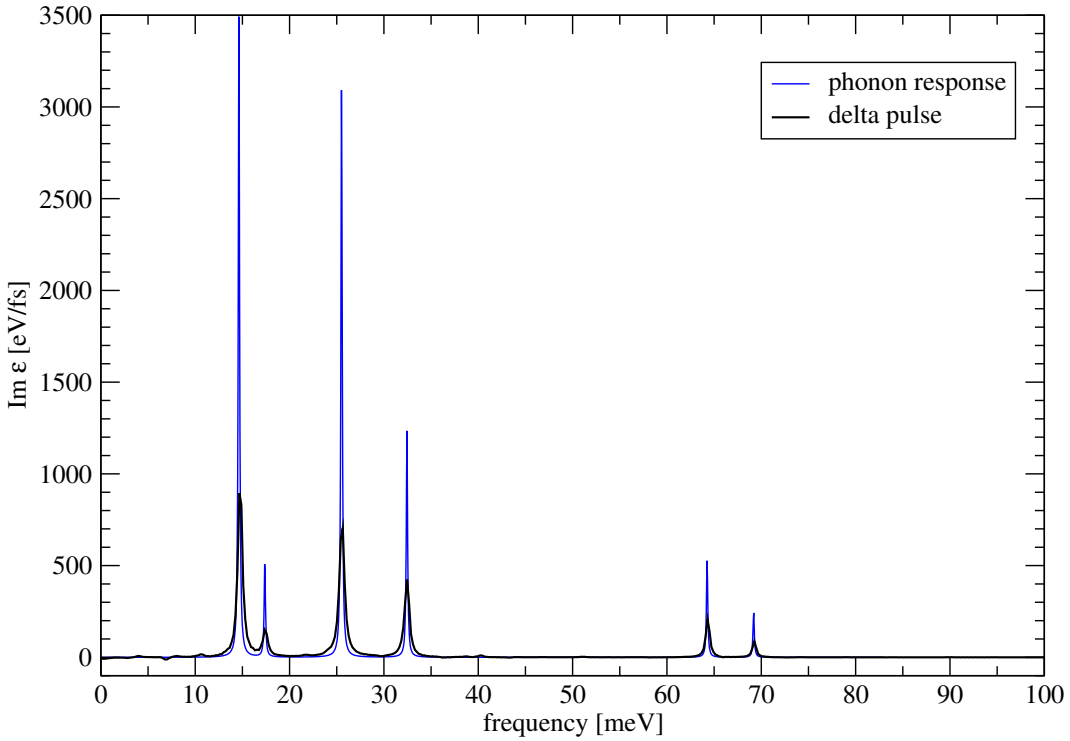

Figure 5.16: Imaginary part of the xx-component of the dielectric tensor of rhombohedral $SrTiO_3$ at low temperature.

As expected, the delta pulse results for fully relaxed $SrTiO_3$ in the single unit cell coincide with the phonon response function. As before, energy conservation is satisfactory.

Similar to figures 5.10 and 5.11, we want to compare this result to the Kubo polarisability at low temperatures. The phase transition from rhombohedral to orthorhombic STO occurs at roughly 100 K, which is why we expect good results from the Kubo run at 10 K.

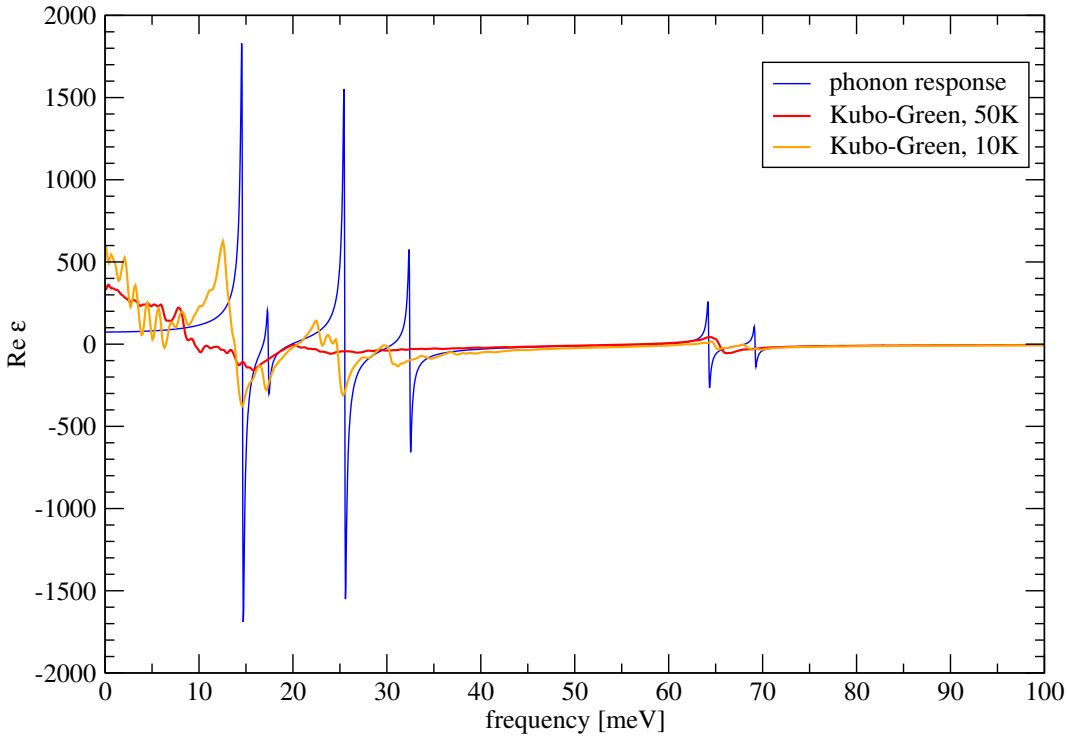

Figure 5.17: Real part of the xx-component of the dielectric tensor of $SrTiO_3$ at low temperatures.

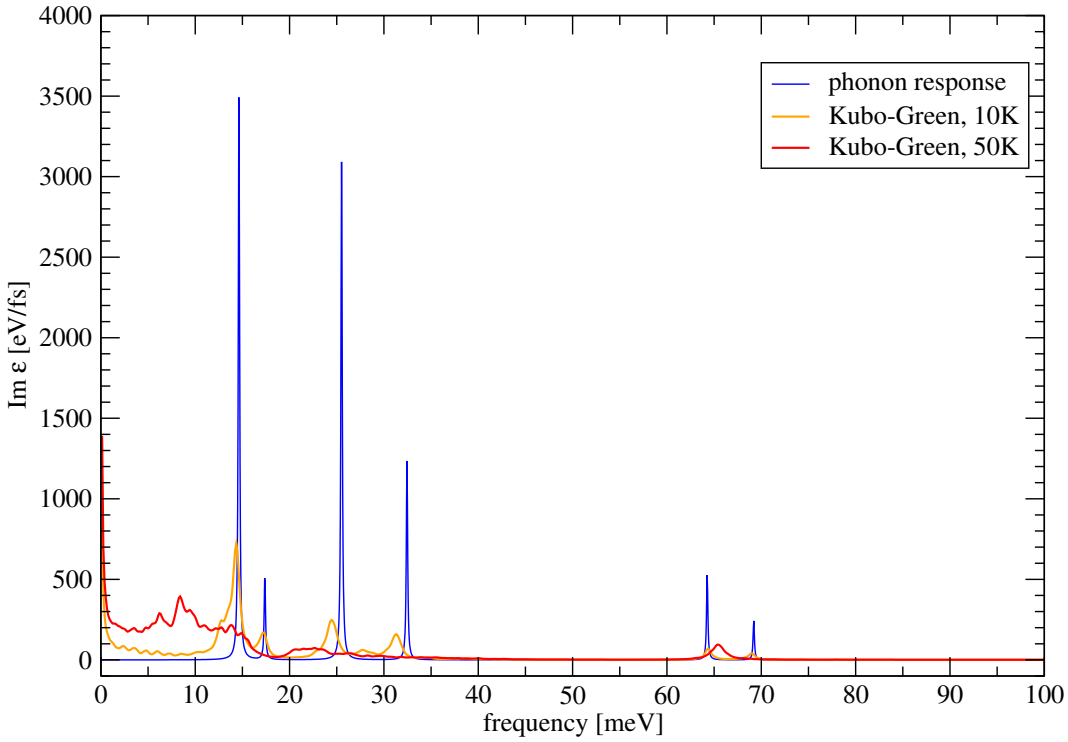

Figure 5.18: Imaginary part of the xx-component of the dielectric tensor of $SrTiO_3$ at low temperatures.

Comparing figures 5.17 and 5.18 with 5.10 and 5.11, we observe that in $SrTiO_3$, anharmonic effects even at temperatures far below the first phase transition play a very important role. Both the real and the imaginary part of the Kubo-Green solution at 50 K have very little to do with the ground-state polarisability obtained from the phonon response. We can attribute this to the pronounced instabilites in the structure.

The $SrTiO_3$ structure posses multiple local minima very close to the global lowest energy structure. Specifically, further ferroelectric distortions e.g. with the Ti and O atoms moving in the +x and -x direction by about 0.1 Åcan occur. These structures are local minima with a slighlty greater energy than the groundstate structure.

Even at 10 K, if the simulations are run long enough, transitions from the global minimum into these local higher energy minima can occur. Typically this is accompanied by a recrossing into the lower energy structure after several picoseconds. Whenever such a transition occurs, the Fourier transform of the dipole-dipole correlation function shows oddities, for instance a strong shift in the peaks.

For the evaluation of the final spectral function, we have removed all trajectories where such a transition took place. Still the spectrum shows a singular peak around ω=0, indicating a very soft global energy mimimum.

To conclude this section, we consider another Kubo-Green dielectric function for $SrTiO_3$, this time obtained in a $2 \times 2 \times 2$ supercell. In figure 5.20, we see the difference between a Kubo run in the single unit cell and the supercell. As for $BaTiO_3$, the results for the unit cell and the supercell are qualitatively very different. In the $2\times2\times2$ supercell, the anti-ferroelectric distorsions are possible, and neighbouring octahedra can perform clockwise/anti-clockwise rotations. In the supercell, we observe a single low-frequency peak, as well as another one at 67 meV.

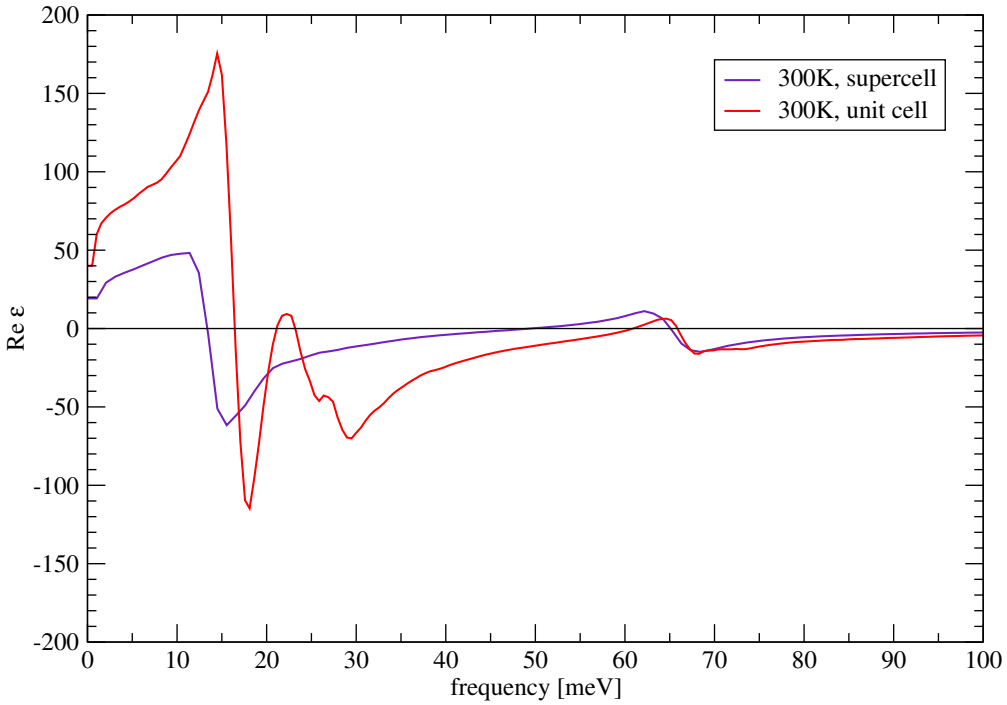

Figure 5.19: Real part of the xx-component of the dielectric tensor of cubic $SrTiO_3$ at high temperature.

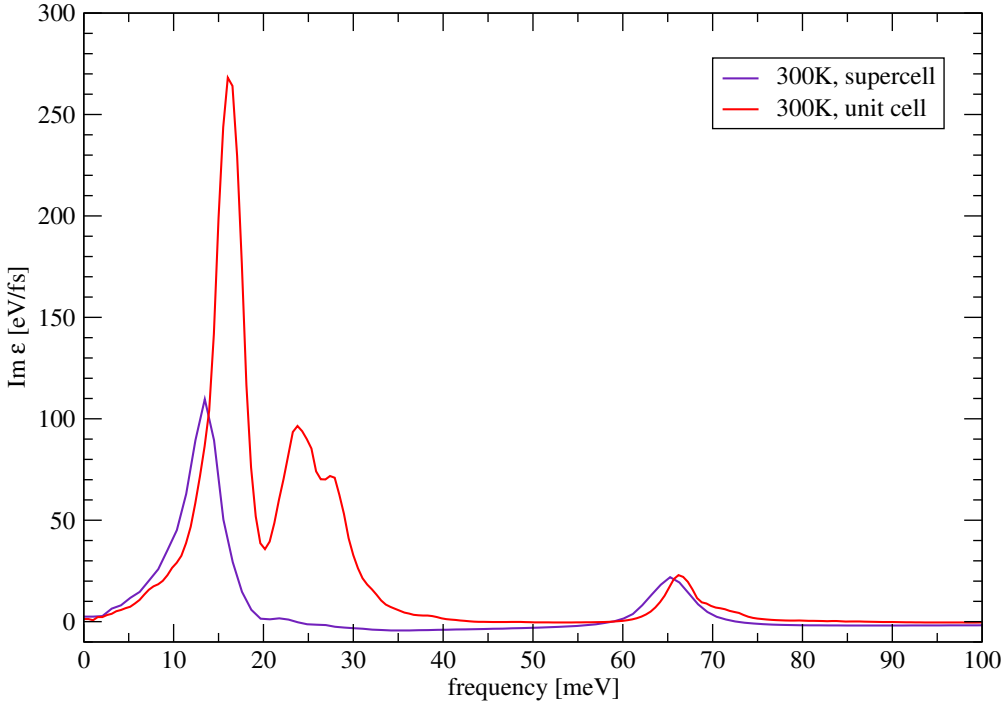

Figure 5.20: Imaginary part of the xx-component of the dielectric tensor of cubic $SrTiO_3$ at high temperature.

Chapter 6

Conclusion

Starting from very simple theoretical considerations on time-dependent perturbation theory, we have presented two derivations of the fluctuation-dissipation theorem. This theorem has been the starting point for obtaining the Kubo-Green relation for the frequency-dependent dielectric tensor of polarisable materials. We have shown that the usual phonon response function can be obtained as a limiting case of the Kubo-Green relation and presented the delta pulse method, in which a special form of perturbation helps to significantly reduce the computional expenses of Kubo-Green.

In the subsequent calculations, we have shown that the three presented approaches, Kubo-Green, delta pulse and phonon response, can be used in a complementary fashion to further the understanding of dielectric properties of materials.

Although computationally rather expensive, the Kubo-Green method allows us to describe dielectric properties at non-zero temperatures up to linear order. Even more importantly, we are also able to describe the polarisability of structurally instable systems, such as barium titanate and strontium titanate. The main complication in these cases stems from the fact that their potential energy landscape is very flat and exhibits several local minima around the global minimum. At higher temperatures, the structure assumes a series of different configurations with different dielectric properties. This implies that in order to compute the polarisability at higher temperatures we need to average over this series of dielectric functions. For sufficiently long runtimes - and sufficiently good statistics - this is achieved by Kubo-Green.

In the limit of low but non-zero temperatures, the delta pulse method can give reliable results at a much lower cost than Kubo-Green. However, the delta pulse can only give reliable results if the system is perfectly stable and does not exhibit very soft modes. In our test system, SiO_2, whose energy landscape is harmonic up to relatively high temperatures, we have been able to reproduce the results of the phonon response with very high accuracy. In most systems, however, this method requires a fair amount of testing, as anharmonic effects can arise as a consequence of the finite size of the electric pulse. This can introduce features to the dielectric function which do not appear within the harmonic approximation.

Lastly, in the groundstate, the phonon response is the method of choice provided that the system is stable. In the presence of negative phonon modes, the results for the phonon response can generally not be trusted. Also, for many applications, the polarisability of a material at the groundstate is not particularly insightful, as phase transitions can severly alter the ionic polarisability.

Using Kubo-Green, we have been able to describe the evolution of the polarisability as a function of temperature for both barium titanate and strontium titanate. The low-temperature results for

the rhombohedral phase in both systems are very close to the polarisability at the ground state. In the cubic phase at higher temperatures, however, many small-scale features get lost and the dipole active modes tend to become softer. The latter can at least in part be attributed to the structural weakness of both compounds. This is most obvious in the case of cubic strontium titanate, which in a larger supercell exhibits further structural instabilities, known as anti-ferroelectric distorsion.

Kubo-Green can be the entry point to a vast field of possible subsequent investigations of the dielectric properties of diverse types of materials. With our small selection of test systems, we were barely able to scrape the surface of what would be very well possible - and even rather easily realisable.

Bibliography

[1] R. Kubo. Statistical-mechanical theory of irreversible processes i. *Journal of the Physical Society of Japan*, 12(6):570–586, 1957.

[2] R Zwanzig. Time-correlation functions and transport coefficients in statistical mechanics. *Annual Review of Physical Chemistry*, 16(1):67–102, 1965.

[3] J.J. Sakurai. *Modern quantum mechanics*. Boston: Addison-Wesley, revised edition, 1994.

[4] R. Gross and A. Marx. *Festkörperphysik*. Berlin: W. de Gruyter, second edition, 2014. German version.

[5] X. Wu, D. Vanderbilt, and D.R. Hamann. Systematic treatment of displacements, strains, and electric fields in density-functional perturbation theory. *Phys. Rev. B*, 72(3):035105, Jul 2005.

[6] D. Sangalli, A. Marini, and A. Debernardi. Pseudopotential-based first-principles approach to the magneto-optical kerr effect: From metals to the inclusion of local fields and excitonic effects. *Phys. Rev. B*, 86:125139, Sep 2012.

[7] M. Bokdam, T. Sander, A. Stroppa, S. Picozzi, D. D. Sarma, C. Franchini, and G. Kresse. Role of polar phonons in the photo excited state of metal halide perovskites. *Scientific Reports*, 6:28618, June 2016.

[8] G. Kresse and J. Hafner. Ab-initio molecular dynamics for liquid metals. *Phys. Rev. B*, 47:558–561, Jan 1993.

[9] G. Kresse and J. Furthmüller. Efficiency of ab-initio total energy calculations for metals and semiconductors using a plane-wave basis set. *Computational Materials Science*, 6(1):15–50, 1996.

[10] G. Kresse and J. Furthmüller. Efficient iterative schemes for ab initio total-energy calculations using a plane-wave basis set. *Phys. Rev. B*, 54:11169–11186, Oct 1996.

[11] K. Momma and F Izumi. Vesta: a three-dimensional visualization system for electronic and structural analysis. *Journal of Applied Crystallography*, 41:653–658, 2008.

[12] G. Kresse, M. Marsman, L.E. Hintzsche, and E. Flage-Larsen. Optical and electronic properties of Si_3N_4 and α-SiO_2. *Phys. Rev. B*, 85:045205, Jan 2012.

[13] G.H. Kwei, A.C. Lawson, and S.J.L. Billinge. Structures of the ferroelectric phases of barium titanate. *J.Phys. Chem*, 97:2368–2377, 1993.

[14] R. Wahl, D. Vogtenhuber, and G. Kresse. $SrTiO_3$ and $BaTiO_3$ revisited using the projector augmented wave method: Performance of hybrid and semilocal functionals. *Phys. Rev. B*, 78:104116, 09 2008.